

UV/IR Mixing in Marginal Fermi Liquids

Weicheng Ye,^{1,2} Sung-Sik Lee,^{1,3} and Liujun Zou¹

¹*Perimeter Institute for Theoretical Physics, Waterloo, Ontario, Canada N2L 2Y5*

²*Department of Physics and Astronomy, University of Waterloo, Waterloo, Ontario, Canada N2L 3G1*

³*Department of Physics and Astronomy, McMaster University, Hamilton, Ontario, Canada L8S 4M1*

When Fermi surfaces (FS) are subject to long-range interactions that are marginal in the renormalization-group sense, Landau Fermi liquids are destroyed, but only barely. With the interaction further screened by particle-hole excitations through one-loop quantum corrections, it has been believed that these marginal Fermi liquids (MFLs) are described by weakly coupled field theories at low energies. In this paper, we point out a possibility in which higher-loop processes qualitatively change the picture through UV/IR mixing, in which the size of FS enters as a relevant scale. The UV/IR mixing effect enhances the coupling at low energies, such that the basin of attraction for the weakly coupled fixed point of a (2+1)-dimensional MFL shrinks to a measure-zero set in the low-energy limit. This UV/IR mixing is caused by gapless virtual Cooper pairs that spread over the entire FS through marginal long-range interactions. Our finding signals a possible breakdown of the patch description for the MFL, and questions the validity of using the MFL as the base theory in a controlled scheme for non-Fermi liquids that arise from relevant long-range interactions.

Introduction. Non-Fermi liquids (nFLs) arise ubiquitously when Fermi surfaces (FS) are coupled to gapless collective modes that mediate long-range interactions. The physics of nFLs is central to the strange metallic behavior and/or unconventional superconductivity in various systems, including cuprates, heavy-fermion compounds, half-filled Landau level and pnictides [1–3]. However, understanding nFLs has been a long-standing challenge due to strong quantum fluctuations amplified by abundant gapless modes near FS [4–9].

Under renormalization group (RG) flow, most theories for (2+1)-dimensional nFLs flow to the strong-coupling regime at low energies, and non-perturbative methods are required to understand their universal long-distance physics [10, 11]. However, there is a special class of nFLs, marginal Fermi liquids (MFLs)¹, where interaction effects are relatively weak, i.e., marginal in the RG sense with logarithmic (log) perturbative corrections. If the marginal interactions are further screened, the long-distance physics should be captured by weakly coupled theories. While the MFL was first introduced for cuprates [12], it is relevant in rather broad contexts. First, metallic states realized at the half-filled Landau level and exotic Mott transitions may be related to MFLs [13, 14]. Second, MFLs have been used as a foothold to gain a controlled access to strongly coupled nFLs in an expansion scheme, where the exponent with which long-range interactions decay in space is used as a control parameter [15, 16].

In nFLs, fermionic quasiparticles are destroyed by scatterings that are singularly enhanced at small momenta. If large-momentum scatterings are suppressed

strongly enough, one can understand physical observables that are local in momentum space (e.g., the single-particle spectral function) within local patches of FS that include the momentum point of interest (see Fig. 1). Although this patch description becomes ultimately invalid in the presence of a pairing instability driven by short-range four-fermion couplings, which is *non-local* in momentum space, one may hope that the dominant physics in the normal state can be captured within the patch theory without invoking the entire FS. So the patch theory [8, 9, 16–18] has been widely used to describe a large class of nFLs (see Refs. [13, 14, 19, 20] for some prominent examples).

In MFLs, however, the validity of the patch theory is questionable even before taking into account the short-range four-fermion couplings, because large-momentum scatterings are only marginally suppressed. If large-momentum scatterings create significant inter-patch couplings, the patch theory fails even for the purpose of describing observables local in momentum space. In this case, the size of the FS, a UV parameter, qualitatively modifies the IR scaling behavior, showcasing UV/IR mixing.

While such UV/IR mixing does not show up at low orders in the perturbative expansion [16, 18], a systematic understanding of higher-order effects is still lacking. This issue is also pertinent to multiple experimentally relevant problems. First, in the context of quantum Hall physics, it is debated whether the Halperin-Lee-Read theory [13] and the recently proposed Son’s theory [21] describe the same universal physics of the composite Fermi liquid (CFL). Second, in the continuous Mott transitions reported in κ -(ET)₂Cu₂(CN)₃ [22, 23] and moiré materials [24, 25], the observed phenomena appear to be compatible with the predictions of the patch theory [14], but some specific critical properties seem to disagree [24]. To resolve these issues,

¹ In this paper, the terms “metal”, “nFL” and “MFL” may refer to that of either electrons or some emergent fermions, depending on the context.

it is crucial to understand the behaviors of the corresponding MFL theories. Moreover, understanding higher-order effects in nFLs in general may provide new insight on the nature of quantum phase transitions associated with sudden jumps of the FS size [26, 27], and deconfined metallic quantum criticality [28–31].

In this paper, we study the higher-order behaviors of a theory of N flavors of two-dimensional FS coupled to a dynamical $U(1)$ gauge field, whose kinetic energy scales as $k_y^{1+\epsilon}$. For the marginal exponent ($\epsilon = 0$), we indeed find potential UV/IR mixing in four-loop processes that renormalize the gauge coupling (see Fig. 2), with a strength logarithmically singular in the FS size. This is caused by gapless *virtual* Cooper pairs that manage to explore the entire FS, assisted by large-momentum scatterings that are only marginally suppressed.

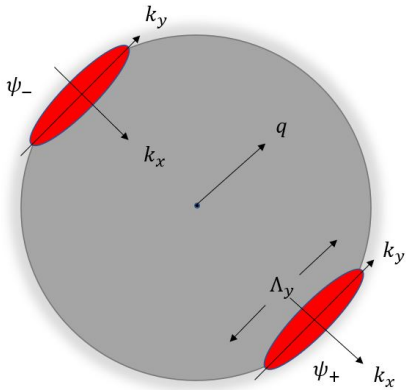


FIG. 1: In the patch theory, a FS is partitioned into multiple patches ($\sim k_F/\Lambda_y$ of them, with k_F the Fermi momentum and Λ_y the patch size). Ignoring the short-range four-fermion interactions, couplings between modes from different patches are weak unless they have almost parallel Fermi velocities. In this case, one can focus on a pair of antipodal patches that have nearly collinear Fermi velocities.

Model and regularization scheme. We denote the low-energy fermion fields near a pair of antipodal patches by ψ_{ip} , with $p = \pm$ the patch index and $i = 1, \dots, N$ the flavor index. a represents the gauge field (see Fig. 1). Due to the kinematic constraints, the most important interactions occur between fermionic modes and the gauge bosons with momenta nearly perpendicular to their Fermi velocity [4, 17]. The Euclidean action for the patch theory is [16]

$$S = S_\psi + S_{\text{int}} + S_a, \quad (1)$$

where

$$S_\psi = \int [dk] \sum_{i,p} \psi_{ip}^\dagger(k) (-ik_\tau + pk_x + k_y^2) \psi_{ip}(k),$$

$$S_{\text{int}} = \int [dk_1][dk_2] \sum_{i,p} \lambda_p a(k_1) \psi_{ip}^\dagger(k_1 + k_2) \psi_{ip}(k_2), \quad (2)$$

$$S_a = \int [dk] \frac{N}{2e^2} |k_y|^{1+\epsilon} a(-k) a(k),$$

with $[dk] = \frac{dk_x dk_y dk_\tau}{(2\pi)^3}$ and $\lambda_\pm = \pm 1$. The reason for the opposite signs of λ_\pm is because a couples to the currents of the fermions, and fermions from the two patches have opposite Fermi velocities. By power counting, the coupling e^2 is marginal (relevant) if $\epsilon = 0$ ($\epsilon > 0$). Physically, with decreasing ϵ , the fermion-boson coupling gets weaker at small momenta, but large-momentum scatterings become stronger, which increases the “risk” of UV/IR mixing. Below we primarily focus on the marginal case with $\epsilon = 0$. Note that a large N is still useful in organizing the calculations when $\epsilon = 0$.

One can introduce two cutoffs. Λ denotes the energy cutoff², and Λ_y is the cutoff of y -momentum. The former is the usual UV cutoff, while the latter represents the size of patch. We take $\Lambda \rightarrow \infty$ for simplicity, i.e., the theory is regularized by Λ_y only. Crucially, Λ_y also serves as IR data that measures the number of gapless modes near the FS, and there is a priori no guarantee that low-energy observables are insensitive to Λ_y . If the Λ_y -dependence cannot be removed in low-energy observables by renormalization, the theory has UV/IR mixing, and the patch description fails.

UV/IR mixing. We consider the photon self-energy, $\Pi(k)$, which is $O(N^1)$ to the leading order. To order N^0 , $\Pi(k)$ is finite as $\Lambda_y \rightarrow \infty$ [9, 16], due to a kinematic constraint that is nevertheless absent at higher orders (see Eq. (30) of the Supplemental Material [32] or [33]). At order N^{-1} , by exact calculations we find a *double-log* divergence in the diagram in Fig. 2a: $\Pi_0(k_\tau = 0, k_y) = \frac{1}{N} \frac{|k_y|}{e^2} \frac{2\alpha^4}{3\pi^2} \left(\ln \left(\frac{\Lambda_y}{k_y} \right) \right)^2$, with $\alpha \equiv e^2/(4\pi)$ (see Sec. III.C.3 in [32]). Other diagrams are harder to compute explicitly. However, under reasonable assumptions, we argue that the only other net contribution to the double-log divergence is from Fig. 2b, whose contribution is also Π_0 at $k_\tau = 0$ (see Sec. III.C.4 in [32]). Double-log divergences are usually from divergences in sub-diagrams, which can then be cancelled by diagrams with counter terms. But the present double-log divergences are not due to

² UV cutoff associated to high-energy modes can be imposed on the x -momentum relative to the FS as well, yet this cutoff violates an emergent gauge invariance [16].

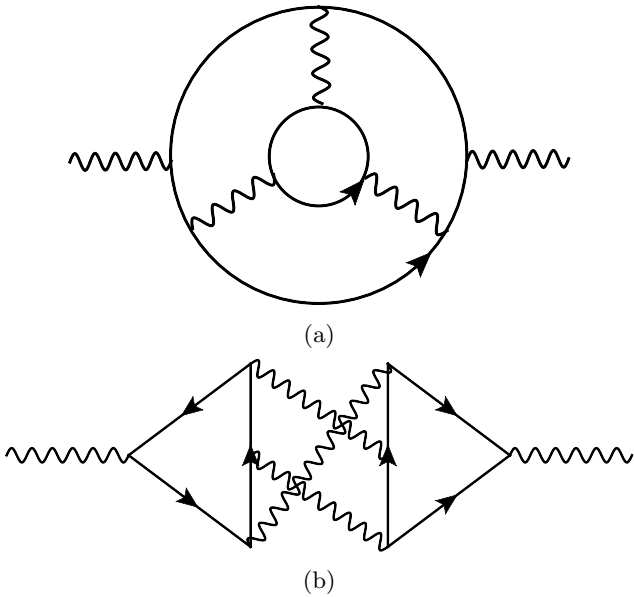


FIG. 2: Eq. (3) comes from these two diagrams, together with their cousins with both internal fermion loops flipped in direction, which are not shown here. Note that only when the two fermion loops in each diagram run in the same direction do they contribute to double-log divergence. See Sec. III.C.2 in [32] for all diagrams at this order.

this, since the only divergent sub-diagram in Fig. 2 is the three-loop vertex correction, but the corresponding counter term does not contribute to the renormalization of the boson kinetic term to order N^{-1} . Taken all diagrams together (including the ones with counter terms), the total double-log divergence to order N^{-1} is

$$\Pi(k_\tau = 0, k_y) \sim \frac{1}{N} \frac{|k_y|}{e^2} \frac{4\alpha^4}{3\pi^2} \left(\ln \left(\frac{\Lambda_y}{k_y} \right) \right)^2. \quad (3)$$

To better understand this result, first consider the usual renormalizable field theories without a FS, e.g., $3+1$ dimensional ϕ^4 theory. In such theories, given a UV cutoff Λ , quantities like $d\Pi/d\ln\Lambda$ are analytic in the external momentum $k \ll \Lambda$, since this derivative measures the contribution of *high-energy* modes in the energy window $[\Lambda, \Lambda + d\Lambda]$ (see Fig. 3). Consequently, the non-analyticity in Π can at most take the form of $k^2 \ln \frac{\Lambda}{k}$, and the Λ -dependence of the results can then be eliminated by local counter terms, allowing any observable at a scale $k_1 \ll \Lambda$ to be expressed solely in terms of renormalized quantities measured at another scale $k_2 \ll \Lambda$, and the IR physics is insensitive to the UV physics.

However, the present theory has another short-distance scale, Λ_y , which measures the number of *gapless* modes near the FS. Low-energy observables in gen-

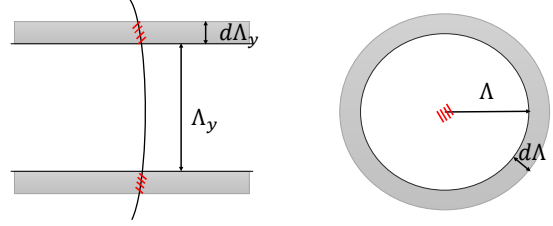


FIG. 3: The gray regions illustrate modes that are integrated out *if* we tune Λ_y in MFL (left) or Λ in a usual field theory without FS (right). The latter has gapless modes only at a single point in the momentum space (shown in red), while the former has gapless modes overlapping with the gray regions. In MFL, $\Pi(k)$ calculated at a *fixed* Λ_y can have IR singularities stronger than $\ln(\Lambda_y/k)$.

eral can depend on Λ_y in a sensitive manner. Especially, $d\Pi/d\ln\Lambda_y$ does not have to be analytic in k (see Fig. 3). Gapless modes can not only renormalize the existing non-local term through $|k_y| \ln(\Lambda_y/|k_y|)$, but also generate stronger non-analyticity in the quantum effective action, such as $|k_y| \ln^n(\Lambda_y/|k_y|)$ with $n > 1$ ($n = 2$ in Eq. (3)). In this case, the Λ_y -dependence cannot be removed in low-energy observables through renormalization of the existing terms (local or not) in the action, signaling UV/IR mixing.

UV/IR mixing is known to arise in metals³. First, the FS size k_F , a UV parameter, becomes relevant at low energies when a critical boson is coupled with FS whose dimension is greater than one, as a boson can decay into particle-hole pairs along the “great circle” of FS whose tangent space includes the boson momentum [39, 40]. Second, the FS size is important in the presence of pairing instabilities driven by short-range four-fermion interactions, via which Cooper pairs residing on the FS with zero total momentum can be scattered throughout the entire FS without violating momentum or energy conservation [18, 41, 42].

The origin of the UV/IR mixing we find here is related to the second one but different. The contribution in Eq. (3) comes from *virtual* Cooper pairs (VCP), represented by the two fermion loops that come from opposite patches and run in the same direction in Fig. 2. Via the *marginal* long-range interactions mediated by the gauge field, these VCP spread over the entire FS, which enjoys a large phase space for scattering and

³ We note that UV/IR mixing with different origins is also proposed in other setups [34–38].

can have singular contributions (see Eq. (86) in [32]). Indeed, the double-log divergence disappears if either the VCP are absent (e.g., by taking the fermion loops in Fig. 2 to be in the same patch and/or run in opposite directions), or large-momentum scatterings are further suppressed (e.g., by taking $\epsilon > 0$)⁴. This is reminiscent to the enhanced quasiparticle decay rate due to VCP in Fermi liquids [45].

Consequences of UV/IR mixing. Eq. (3) forces us to view Λ_y as another *coupling constant* of the theory [39]. In particular, $\tilde{\Lambda}_y \equiv \Lambda_y/\mu$ plays the role of a relevant coupling as the size of FS blows up relative to the decreasing scale μ . The beta functions of the theory are (see Sec. I and II in [32] for details)

$$\frac{d\tilde{\Lambda}_y}{d\ln\mu} = -\tilde{\Lambda}_y, \quad \frac{d\alpha}{d\ln\mu} = \frac{2\alpha^2}{\pi N} - \frac{8\alpha^5}{3\pi^2 N^2} \ln \tilde{\Lambda}_y. \quad (4)$$

Let us analyze these beta functions in the weak-coupling regime with $\alpha \lesssim 1$ and low-energy limit with $\mu \ll \Lambda_y$, together with a large but finite N . The first term in $d\alpha/d\ln\mu$ is the lowest-order term in $1/N$ and $\tilde{\Lambda}_y$ -independent. As the scale μ is lowered, it makes the gauge coupling decrease logarithmically through screening. If the initial coupling α_0 defined at energy scale μ_0 satisfies $(\alpha_0^3/N) \cdot \ln(\Lambda_y/\mu_0) \lesssim 1$, this term dominates and the gauge coupling flows to zero at low energies. On the other hand, for $(\alpha_0^3/N) \cdot \ln(\Lambda_y/\mu_0) \gtrsim 1$, the second term dominates, which tends to enhance the coupling at low energies. In this case, we can ignore the first term to the leading order. Then the gauge coupling grows as $\alpha = \alpha_0 \left[1 - \frac{16}{3\pi^2 N^2} \alpha_0^4 \left(\ln^2 \left(\frac{\mu}{\Lambda_y} \right) - \ln^2 \left(\frac{\mu_0}{\Lambda_y} \right) \right) \right]^{-1/4}$. This solution shows a divergence of the gauge coupling with decreasing μ , although it cannot be trusted in the strong coupling regime. For theories defined at scale μ_0 , the basin of attraction for the $\alpha = 0$ fixed point is given by $\mathcal{B}_{\mu_0} \equiv \{\alpha_0 | \alpha_0^3 < cN/\ln(\Lambda_y/\mu_0)\}$, with c an $O(1)$ constant (see the shaded region in Fig. 4). The salient feature is that \mathcal{B}_{μ_0} shrinks to a measure-zero set in the low-energy limit (i.e., $\mu_0 \ll \Lambda_y$), due to the scale dependence in the beta function. The fact that the beta function explicitly depends on Λ_y is a hallmark of UV/IR mixing.

In the presence of the UV/IR mixing, the FS size cannot be dropped in low-energy physical observables. For example, the single-fermion spectral function takes the form of $\mathcal{A}(\omega, \mathbf{k}, T) = \omega^\Delta f \left(\frac{\omega}{k_\parallel^z}, \frac{k_\parallel}{k_F^{z'}}, \frac{\omega}{T} \right)$, where k_F is

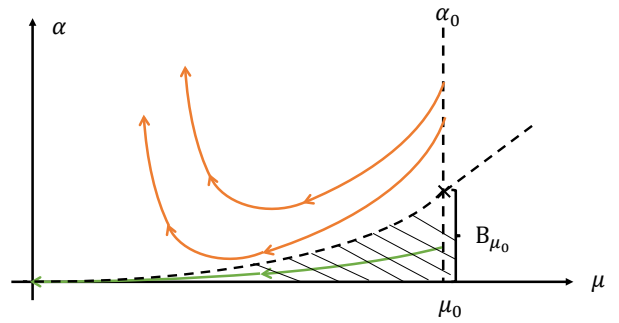


FIG. 4: The flow of $\alpha = e^2/(4\pi)$ with initial condition $\alpha = \alpha_0$ at $\mu = \mu_0$. For each μ_0 , there is a critical value $\alpha^* \approx N/\ln(\Lambda_y/\mu_0)$ (the dashed curve): when $\alpha_0 < \alpha^*$ the gauge coupling flows to zero at low energies (green), while when $\alpha_0 > \alpha^*$ it flows to infinity (orange).

the FS size, k_\parallel is the distance of \mathbf{k} away from the FS, T is the temperature, Δ , z and z' are critical exponents ($z' = 2$ from Eq. (3)), and f is a universal function [39]. It is interesting to test this in CFLs at various filling factors that can be realized in Chern bands [29].

The UV/IR mixing in MFLs also has implications for the ϵ -expansion scheme [15, 16], which has been used to approach nFLs with $\epsilon = 1$ from MFLs with $\epsilon = 0$ perturbatively in ϵ . To see it, we examine how the UV/IR mixing in the base theory with $\epsilon = 0$ affects the perturbative ϵ -expansion. In theories with $\epsilon > 0$, the UV/IR mixing disappears since the diagrams in Fig. 2 are no longer divergent in Λ_y , as large-momentum scatterings are further suppressed. Instead, the double-log in Eq. (3) is translated to a double pole in ϵ as⁵

$$\Pi(k_\tau = 0, k_y) \sim \frac{1}{N} \frac{|k_y|}{\tilde{e}^2} \frac{8\tilde{\alpha}^4}{\pi^2} \times \left(\frac{1}{27\epsilon^2} + \frac{1}{9\epsilon} \ln(\mu/|k_y|) + \frac{1}{6} (\ln(\mu/|k_y|))^2 \right), \quad (5)$$

where $\tilde{e}^2 = e^2\mu^{-\epsilon}$ is the dimensionless coupling and $\tilde{\alpha} = \tilde{e}^2/(4\pi)$. Since $1/\epsilon$ -poles cannot be absorbed by terms already present in the action, the naive perturbative expansion appears ill-defined. Moreover, this singular self-energy suggests that ϵ is renormalized to a larger value, further indicating that the ϵ -expansion may break down. This calls for alternative control schemes for nFLs. See Refs. [47–49] for the dimensional regularization scheme that has no UV/IR mixing, and Refs. [50–53] for other proposals.

Summary and discussion. We provide strong evidence that a $(2+1)$ -dimensional MFL exhibits UV/IR

⁴ Our double-log divergence appears similar to the Sudakov double pole [43, 44] in QED and effective theories of QCD. Both of them originate from gapless degrees of freedom. However, the Sudakov double-log originates from small momentum modes while our double-log divergence is from modes with large y -momentum.

⁵ See Ref. [46] for a different but related calculation at $\epsilon = 1$.

mixing, caused by virtual Cooper pairs that spread over the entire FS due to large-momentum scatterings. Our finding suggests the breakdown of the patch theory for MFLs and a potential issue in the ϵ -expansion that uses MFLs as the base theory for nFLs.

We conclude with a few final remarks. First, the UV/IR mixing identified in $(2+1)$ -dimensional MFLs can be extended to more general cases. Consider metals with m -dimensional FS (e.g., a spherical or cylindrical FS has $m=2$ and a Weyl nodal line has $m=1$) coupled to a critical boson whose kinetic energy goes as $k_y^{1+\epsilon}$. The contribution of virtual Cooper pairs to loop corrections scales as $\sim \int \frac{d^m k_y}{k_y^{1+\epsilon}}$, which suggests that for $m \geq 1 + \epsilon$, there exist UV divergences associated with the extended size of FS, and UV/IR mixing can arise. So we expect virtual-Cooper-pair-induced UV/IR mixing in $(3+1)$ -dimensional gauge theories with $m=2$ and $\epsilon=1$ (on top of the UV/IR mixing identified in Ref. [39]). This is relevant to quantum spin liquids [54, 55] and mixed-valence insulators [56]⁶.

Second, our result is obtained within the standard patch theory. To understand the full consequences of the UV/IR mixing caused by large-momentum scatterings, one should consider a general theory that keeps track of how the boson-fermion coupling is renormalized at *large* boson momenta. For this, instead of a coupling constant, one should take into account a *momentum-dependent coupling function*, reminiscent of the familiar form factors in the interaction vertices in various settings [57]. Moreover, the four-fermion couplings, which should also be described by a coupling function, are not considered here, but they should in principle be studied on equal footing as the gauge coupling. Whether there is UV/IR mixing can depend on the microscopic details of the physical system. What we have shown is the presence of a UV/IR mixing in systems where the two effects above are negligible. In the future, it will be of great interest to understand whether such UV/IR mixing exists in systems where these effects are significant and should be incorporated into the theory. In any case, our results suggest that the physics of MFLs is richer than originally expected, and mandates a qualitative improvement of the current theoretical understanding.

Acknowledgement. We thank Tobias Holder, Subir Sachdev and T. Senthil for helpful discussion. W.Y. would like to especially thank Timothy Hsieh for introducing the topic of non-Fermi liquid, Haoran Jiang for explaining double-log behavior in phenomenology and

Minyong Guo for hospitality during his stay in Beijing where the bulk calculation was carried out. Research at Perimeter Institute is supported in part by the Government of Canada through the Department of Innovation, Science and Economic Development Canada and by the Province of Ontario through the Ministry of Colleges and Universities. S.L. acknowledges the support of the Natural Sciences and Engineering Research Council of Canada.

-
- [1] T. Senthil, “On non-Fermi liquid quantum critical points in heavy fermion metals,” *Annals of Physics* **321**, 1669–1681 (2006), arXiv:cond-mat/0604240 [cond-mat.str-el].
 - [2] Sung-Sik Lee, “Recent Developments in Non-Fermi Liquid Theory,” *Annual Review of Condensed Matter Physics* **9**, 227–244 (2018), arXiv:1703.08172 [cond-mat.str-el].
 - [3] Erez Berg, Samuel Lederer, Yoni Schattner, and Simon Trebst, “Monte Carlo Studies of Quantum Critical Metals,” *Annual Review of Condensed Matter Physics* **10**, 63–84 (2019), arXiv:1804.01988 [cond-mat.str-el].
 - [4] Joseph Polchinski, “Effective Field Theory and the Fermi Surface,” arXiv e-prints, hep-th/9210046 (1992), arXiv:hep-th/9210046 [hep-th].
 - [5] B. L. Altshuler, L. B. Ioffe, and A. J. Millis, “Low-energy properties of fermions with singular interactions,” *Phys. Rev. B* **50**, 14048–14064 (1994).
 - [6] Yong Baek Kim, Patrick A. Lee, and Xiao-Gang Wen, “Quantum Boltzmann equation of composite fermions interacting with a gauge field,” *Phys. Rev. B* **52**, 17275–17292 (1995), arXiv:cond-mat/9504063 [cond-mat].
 - [7] Ar. Abanov and A. Chubukov, “Anomalous scaling at the quantum critical point in itinerant antiferromagnets,” *Phys. Rev. Lett.* **93**, 255702 (2004).
 - [8] Sung-Sik Lee, “Low-energy effective theory of Fermi surface coupled with U(1) gauge field in 2+1 dimensions,” *Phys. Rev. B* **80**, 165102 (2009), arXiv:0905.4532 [cond-mat.str-el].
 - [9] Max A. Metlitski and Subir Sachdev, “Quantum phase transitions of metals in two spatial dimensions. I. Ising-nematic order,” *Phys. Rev. B* **82**, 075127 (2010), arXiv:1001.1153 [cond-mat.str-el].
 - [10] Shouvik Sur and Sung-Sik Lee, “Chiral non-Fermi liquids,” *Phys. Rev. B* **90**, 045121 (2014), arXiv:1310.7543 [cond-mat.str-el].
 - [11] Andres Schliefl, Peter Lunts, and Sung-Sik Lee, “Exact critical exponents for the antiferromagnetic quantum critical metal in two dimensions,” *Phys. Rev. X* **7**, 021010 (2017).
 - [12] C. M. Varma, P. B. Littlewood, S. Schmitt-Rink, E. Abrahams, and A. E. Ruckenstein, “Phenomenology of the normal state of Cu-O high-temperature superconductors,” *Phys. Rev. Lett.* **63**, 1996–1999 (1989).
 - [13] B. I. Halperin, Patrick A. Lee, and Nicholas Read, “Theory of the half-filled Landau level,” *Phys. Rev. B* **47**, 7312–7343 (1993).

⁶ Since $\epsilon=1$ corresponds to local kinetic term for gauge boson, we expect that UV/IR mixing identified here does not originate from the non-analyticity of the kinetic term of the gauge boson.

- [14] T. Senthil, “Theory of a continuous Mott transition in two dimensions,” *Phys. Rev. B* **78**, 045109 (2008), [arXiv:0804.1555 \[cond-mat.str-el\]](#).
- [15] Chetan Nayak and Frank Wilczek, “Non-Fermi liquid fixed point in $2 + 1$ dimensions,” *Nuclear Physics B* **417**, 359–373 (1994), [arXiv:cond-mat/9312086 \[cond-mat\]](#).
- [16] David F. Mross, John McGreevy, Hong Liu, and T. Senthil, “Controlled expansion for certain non-Fermi-liquid metals,” *Phys. Rev. B* **82**, 045121 (2010), [arXiv:1003.0894 \[cond-mat.str-el\]](#).
- [17] Sung-Sik Lee, “Stability of the $U(1)$ spin liquid with a spinon Fermi surface in $2+1$ dimensions,” *Phys. Rev. B* **78**, 085129 (2008), [arXiv:0804.3800 \[cond-mat.str-el\]](#).
- [18] Max A. Metlitski, David F. Mross, Subir Sachdev, and T. Senthil, “Cooper pairing in non-fermi liquids,” *Phys. Rev. B* **91**, 115111 (2015).
- [19] Patrick A. Lee and Naoto Nagaosa, “Gauge theory of the normal state of high- T_c superconductors,” *Phys. Rev. B* **46**, 5621–5639 (1992).
- [20] Sung-Sik Lee and Patrick A. Lee, “ $U(1)$ Gauge Theory of the Hubbard Model: Spin Liquid States and Possible Application to κ -(BEDT-TTF) $_2$ Cu $_2$ (CN) $_3$,” *Phys. Rev. Lett.* **95**, 036403 (2005), [arXiv:cond-mat/0502139 \[cond-mat.str-el\]](#).
- [21] Dam Thanh Son, “Is the Composite Fermion a Dirac Particle?” *Physical Review X* **5**, 031027 (2015), [arXiv:1502.03446 \[cond-mat.mes-hall\]](#).
- [22] Y. Kurosaki, Y. Shimizu, K. Miyagawa, K. Kanoda, and G. Saito, “Mott Transition from a Spin Liquid to a Fermi Liquid in the Spin-Frustrated Organic Conductor κ -(ET) $_2$ Cu $_2$ (CN) $_3$,” *Phys. Rev. Lett.* **95**, 177001 (2005), [arXiv:cond-mat/0504273 \[cond-mat.str-el\]](#).
- [23] Tetsuya Furukawa, Kazuya Miyagawa, Hiromi Taniguchi, Reizo Kato, and Kazushi Kanoda, “Quantum criticality of mott transition in organic materials,” *Nature Physics* **11**, 221–224 (2015).
- [24] Tingxin Li, Shengwei Jiang, Lizhong Li, Yang Zhang, Kaifei Kang, Jiacheng Zhu, Kenji Watanabe, Takashi Taniguchi, Debanjan Chowdhury, Liang Fu, Jie Shan, and Kin Fai Mak, “Continuous Mott transition in semiconductor moiré superlattices,” *Nature (London)* **597**, 350–354 (2021), [arXiv:2103.09779 \[cond-mat.str-el\]](#).
- [25] Augusto Ghitto, En-Min Shih, Giancarlo S. S. G. Pereira, Daniel A. Rhodes, Bumho Kim, Jiawei Zang, Andrew J. Millis, Kenji Watanabe, Takashi Taniguchi, James C. Hone, Lei Wang, Cory R. Dean, and Abhay N. Pasupathy, “Quantum criticality in twisted transition metal dichalcogenides,” *Nature (London)* **597**, 345–349 (2021), [arXiv:2103.09796 \[cond-mat.mes-hall\]](#).
- [26] Hiroaki Shishido, Rikio Settai, Hisatomo Harima, and Yoshichika Onuki, “A drastic change of the fermi surface at a critical pressure in cerhin5: dhva study under pressure,” *Journal of the Physical Society of Japan* **74**, 1103–1106 (2005), <https://doi.org/10.1143/JPSJ.74.1103>.
- [27] Yawen Fang, Gael Grissonnanche, Anaëlle Legros, Simon Verret, Francis Laliberte, Clement Collignon, Amirreza Ataei, Maxime Dion, Jianshi Zhou, David Graf, M. J. Lawler, Paul Goddard, Louis Taillefer, and B. J. Ramshaw, “Fermi surface transformation at the pseudogap critical point of a cuprate superconductor,” [arXiv e-prints](#), [arXiv:2004.01725 \(2020\)](#), [arXiv:2004.01725 \[cond-mat.str-el\]](#).
- [28] Liujun Zou and Debanjan Chowdhury, “Deconfined metallic quantum criticality: A $U(2)$ gauge-theoretic approach,” *Physical Review Research* **2**, 023344 (2020), [arXiv:2002.02972 \[cond-mat.str-el\]](#).
- [29] Liujun Zou and Debanjan Chowdhury, “Deconfined Metal-Insulator Transitions in Quantum Hall Bilayers,” *Physical Review Research* **2**, 032071 (2020), [arXiv:2004.14391 \[cond-mat.str-el\]](#).
- [30] Ya-Hui Zhang and Subir Sachdev, “From the pseudogap metal to the Fermi liquid using ancilla qubits,” *Physical Review Research* **2**, 023172 (2020), [arXiv:2001.09159 \[cond-mat.str-el\]](#).
- [31] Ya-Hui Zhang and Subir Sachdev, “Deconfined criticality and ghost Fermi surfaces at the onset of antiferromagnetism in a metal,” *Phys. Rev. B* **102**, 155124 (2020), [arXiv:2006.01140 \[cond-mat.str-el\]](#).
- [32] See the Supplementary Material for additional details of the analysis, and additional references, including Refs. [58, 59].
- [33] Tobias Holder and Walter Metzner, “Fermion loops and improved power-counting in two-dimensional critical metals with singular forward scattering,” *Phys. Rev. B* **92**, 245128 (2015), [arXiv:1509.07783 \[cond-mat.str-el\]](#).
- [34] Sedigh Ghamari, Sung-Sik Lee, and Catherine Kallin, “Renormalization group analysis of a neck-narrowing Lifshitz transition in the presence of weak short-range interactions in two dimensions,” *Phys. Rev. B* **92**, 085112 (2015), [arXiv:1407.6732 \[cond-mat.str-el\]](#).
- [35] Nathan Seiberg and Shu-Heng Shao, “Exotic $U(1)$ symmetries, duality, and fractons in $3+1$ -dimensional quantum field theory,” *SciPost Physics* **9**, 046 (2020), [arXiv:2004.00015 \[cond-mat.str-el\]](#).
- [36] Yizhi You, Julian Bibo, Taylor L. Hughes, and Frank Pollmann, “Fractonic critical point proximate to a higher-order topological insulator: How does UV blend with IR?” [arXiv e-prints](#), [arXiv:2101.01724 \(2021\)](#), [arXiv:2101.01724 \[cond-mat.str-el\]](#).
- [37] Henry Shackleton, Alex Thomson, and Subir Sachdev, “Deconfined criticality and a gapless Z_2 spin liquid in the square-lattice antiferromagnet,” *Phys. Rev. B* **104**, 045110 (2021), [arXiv:2104.09537 \[cond-mat.str-el\]](#).
- [38] Zheng Zhou, Xue-Feng Zhang, Frank Pollmann, and Yizhi You, “Fractal Quantum Phase Transitions: Critical Phenomena Beyond Renormalization,” [arXiv e-prints](#), [arXiv:2105.05851 \(2021\)](#), [arXiv:2105.05851 \[cond-mat.str-el\]](#).
- [39] Ipsita Mandal and Sung-Sik Lee, “Ultraviolet/infrared mixing in non-Fermi liquids,” *Phys. Rev. B* **92**, 035141 (2015), [arXiv:1407.0033 \[cond-mat.str-el\]](#).
- [40] Ipsita Mandal, “UV/IR mixing in non-Fermi liquids: higher-loop corrections in different energy ranges,” *European Physical Journal B* **89**, 278 (2016), [arXiv:1608.06642 \[cond-mat.str-el\]](#).
- [41] Leon N. Cooper, “Bound electron pairs in a degenerate fermi gas,” *Phys. Rev.* **104**, 1189–1190 (1956).
- [42] Huajia Wang, Srinivas Raghu, and Gonzalo Torroba, “Non-Fermi-liquid superconductivity: Eliashberg approach versus the renormalization group,” *Phys. Rev. B* **95**, 165137 (2017), [arXiv:1612.01971 \[cond-mat.str-el\]](#).
- [43] Michael E. Peskin and Daniel V. Schroeder, *An Introduction to quantum field theory* (Addison-Wesley,

- Reading, USA, 1995).
- [44] Iain Stewart, 8.851 Effective Field Theory. Spring 2013. Massachusetts Institute of Technology: MIT OpenCourseWare, <https://ocw.mit.edu/courses/physics/8-851-effective-field-theory-spring-2013/>. License: Creative Commons BY-NC-SA.
- [45] Dimitri Pimenov, Alex Kamenev, and Andrey V. Chubukov, “One-dimensional scattering of two-dimensional fermions near quantum criticality,” *Phys. Rev. B* **103**, 214519 (2021), arXiv:2104.13802 [cond-mat.str-el].
- [46] Tobias Holder and Walter Metzner, “Anomalous dynamical scaling from nematic and U(1) gauge field fluctuations in two-dimensional metals,” *Phys. Rev. B* **92**, 041112 (2015), arXiv:1503.05089 [cond-mat.str-el].
- [47] Denis Dalidovich and Sung-Sik Lee, “Perturbative non-Fermi liquids from dimensional regularization,” *Phys. Rev. B* **88**, 245106 (2013), arXiv:1307.3170 [cond-mat.str-el].
- [48] Shouvik Sur and Sung-Sik Lee, “Quasilocal strange metal,” *Phys. Rev. B* **91**, 125136 (2015), arXiv:1405.7357 [cond-mat.str-el].
- [49] Peter Lunts, Andres Schliefl, and Sung-Sik Lee, “Emergence of a control parameter for the antiferromagnetic quantum critical metal,” *Phys. Rev. B* **95**, 245109 (2017), arXiv:1701.08218 [cond-mat.str-el].
- [50] Jeremias Aguilera Damia, Shamit Kachru, Srinivas Raghu, and Gonzalo Torroba, “Two dimensional non-Fermi liquid metals: a solvable large N limit,” *Phys. Rev. Lett.* **123**, 096402 (2019), arXiv:1905.08256 [cond-mat.str-el].
- [51] Erik E. Aldape, Taylor Cookmeyer, Aavishkar A. Patel, and Ehud Altman, “Solvable Theory of a Strange Metal at the Breakdown of a Heavy Fermi Liquid,” arXiv e-prints, arXiv:2012.00763 (2020), arXiv:2012.00763 [cond-mat.str-el].
- [52] Jaewon Kim, Ehud Altman, and Xiangyu Cao, “Dirac fast scramblers,” *Phys. Rev. B* **103**, L081113 (2021), arXiv:2010.10545 [cond-mat.str-el].
- [53] Ilya Esterlis, Haoyu Guo, Aavishkar A. Patel, and Subir Sachdev, “Large-N theory of critical Fermi surfaces,” *Phys. Rev. B* **103**, 235129 (2021), arXiv:2103.08615 [cond-mat.str-el].
- [54] Yi Zhou, Patrick A. Lee, Tai-Kai Ng, and Fu-Chun Zhang, “Na₄Ir₃O₈ as a 3D Spin Liquid with Fermionic Spinons,” *Phys. Rev. Lett.* **101**, 197201 (2008), arXiv:0806.3323 [cond-mat.str-el].
- [55] Michael J. Lawler, Arun Paramekanti, Yong Baek Kim, and Leon Balents, “Gapless Spin Liquids on the Three-Dimensional Hyperkagome Lattice of Na₄Ir₃O₈,” *Phys. Rev. Lett.* **101**, 197202 (2008), arXiv:0806.4395 [cond-mat.str-el].
- [56] Debanjan Chowdhury, Inti Sodemann, and T. Senthil, “Mixed-valence insulators with neutral Fermi surfaces,” *Nature Communications* **9**, 1766 (2018), arXiv:1706.00418 [cond-mat.str-el].
- [57] Siddharth A. Parameswaran, Rahul Roy, and Shivaji L. Sondhi, “Fractional quantum Hall physics in topological flat bands,” *Comptes Rendus Physique* **14**, 816–839 (2013), arXiv:1302.6606 [cond-mat.str-el].
- [58] R. Shankar, “Renormalization-group approach to interacting fermions,” *Reviews of Modern Physics* **66**, 129–192 (1994), arXiv:cond-mat/9307009 [cond-mat].
- [59] L. G. Aslamazov and A. I. Larkin, “Effect of Fluctuations on the Properties of a Superconductor Above the Critical Temperature - Sov. Phys. Solid State 10, 875 (1968),” in *30 Years of the Landau Institute*, Vol. 11, edited by Isaak M. Khalatnikov and Vladimir P. Mineev (1996) p. 23.

Supplemental Material for “UV/IR Mixing in Marginal Fermi Liquids”

Weicheng Ye,^{1,2} Sung-Sik Lee,^{1,3} and Liujun Zou¹

¹*Perimeter Institute for Theoretical Physics, Waterloo, Ontario, Canada N2L 2Y5*

²*Department of Physics and Astronomy, University of Waterloo, Waterloo, Ontario, Canada N2L 3G1*

³*Department of Physics and Astronomy, McMaster University, Hamilton, Ontario, Canada L8S 4M1*

Contents

I. Framework for Renormalization Group Analysis	1
II. Summary of the RG Results	4
III. Feynman Diagram Calculations	4
A. Second Leading Order Result of Self-Energy	5
B. Third Leading Order Result of Fermion Self-Energy	7
C. Third leading Order Result of Boson Self-Energy	10
1. General Strategies of Calculation and Assumptions	10
2. All Diagrams at the Third Leading Order	12
3. Benz Diagram	12
4. 3-String Diagram	17
References	22

This Supplemental Material contains the framework for the renormalization group (RG) analysis (Section I), a summary of the RG results (Section II), and the details of the Feynman diagram calculations (Section III).

I. Framework for Renormalization Group Analysis

In this section, we present the framework for our field-theoretic RG analysis. In terms of the renormalized fields and couplings, the action of the patch theory for N Fermi surfaces (FS) coupled to a $U(1)$ gauge field is written as

$$S = S_\psi + S_{\text{int}} + S_a, \quad (1)$$

where

$$\begin{aligned} S_\psi &= \int [dk] \sum_{i,p} \psi_{ip}^\dagger(k) [-iZ_1 k_\tau + Z_2(pk_x + k_y^2)] \psi_{ip}(k), \\ S_{\text{int}} &= \int [dk_1][dk_2] \sum_{i,p} Z_2 \lambda_p a(-k_1) \psi_{ip}^\dagger(k_2) \psi_{ip}(k_1 + k_2), \\ S_a &= \int [dk] Z_3 \frac{N}{2e^2 \mu^\epsilon} |k_y|^{1+\epsilon} a(-k) a(k) \end{aligned} \quad (2)$$

with $[dk] \equiv \frac{dk_\tau dk_x dk_y}{(2\pi)^3}$, $\lambda_\pm = \pm 1$, μ a renormalization scale with the same dimension as k_y , and $Z_{1,2,3}$ some renormalization factors. In the above, the rotational symmetry of the patch theory is invoked for the absence of the relative renormalization between k_x and k_y^2 , and the Ward identity is used to guarantee that the multiplicative renormalization of S_{int} is the same as that of $(pk_x + k_y^2)$ part of the fermion kinetic term [1]. For latter convenience, define $\alpha \equiv \gamma e^2$ with $\gamma \equiv 1/(4\pi)$ as a proxy for the coupling constant e^2 . The renormalized fields, couplings and

momentum are related to the bare ones via

$$\begin{aligned} k_{\tau B} &= \frac{Z_1}{Z_2} k_\tau \equiv Z_\tau k_\tau, \quad k_{xB} = k_x, \quad k_{yB} = k_y, \\ \psi_{ipB}(k_B) &= \sqrt{\frac{Z_2}{Z_\tau}} \psi_{ip}(k) \equiv \sqrt{Z_\psi} \psi_{ip}(k), \quad a_B(k_B) = \frac{1}{Z_\tau} a(k) \equiv \sqrt{Z_a} a(k), \\ \alpha_B &\equiv \gamma e_B^2 = \frac{1}{Z_3 Z_\tau} \gamma e^2 \mu^\epsilon \equiv Z_\alpha \alpha \mu^\epsilon \end{aligned} \quad (3)$$

where the subscript B stands for bare. Z_τ is introduced to account for a nontrivial dynamical exponent, Z_ψ and Z_a are introduced to account for anomalous dimensions of the fermion and gauge fields, respectively, and Z_α is introduced to account for the flow of α . At the tree level, the fields and couplings have the following scaling dimensions in momentum space:

$$\begin{aligned} [k_\tau]_0 &= 2, \quad [k_x]_0 = 2, \quad [k_y]_0 = 1, \\ [\psi_{ip}(k)]_0 &= -\frac{7}{2}, \quad [a(k)]_0 = -3, \quad [e^2]_0 = 0. \end{aligned} \quad (4)$$

The Z factors are chosen so that the following renormalization conditions are satisfied:

$$\begin{aligned} \frac{\partial \Sigma(k_\tau = \mu^2, k_x = k_y = 0)}{\partial k_\tau} &= 0, \\ \Sigma(k_y = \mu, k_\tau = k_x = 0) &= 0, \\ \Pi(k_y = \mu, k_\tau = k_x = 0) &= 0, \end{aligned} \quad (5)$$

where Σ and Π are the 1-particle irreducible self-energy of the renormalized fermionic and gauge fields, respectively, and μ is the renormalization scale. Below we focus on the case with $\epsilon = 0$. In this case, it turns out that physical observables have divergence as Λ_y , the cutoff of k_y , goes to infinity. Notice that Λ_y measures the abundance of *gapless* degrees of freedom (DOF) on the FS, so it is not a cutoff as in a usual field theory, which separates high-energy DOF from low-energy ones. Accordingly, it is more appropriate to view Λ_y as a parameter that is on equal footing as the couplings of the theory.

Denote a correlation function involving n_ψ fermionic fields and n_a gauge fields by $G^{(n_\psi, n_a)}$, which is generically written as a function of a set of momenta, α , μ and Λ_y . Then $G_B^{(n_\psi, n_a)} \cdot \delta(\{k_B\}) = Z_\psi^{\frac{n_\psi}{2}} Z_a^{\frac{n_a}{2}} G^{(n_\psi, n_a)}(\{k\}) \cdot \delta(\{k\})$, where $\{k\}$ denotes the momenta this correlation function depends on, and the δ -functions impose momentum conservation. Due to $k_{\tau B} = Z_\tau k_\tau$, $\delta(\{k\}) = Z_\tau \delta(\{k_B\})$, $G_B^{(n_\psi, n_a)} = Z_\psi^{\frac{n_\psi}{2}} Z_a^{\frac{n_a}{2}} Z_\tau G^{(n_\psi, n_a)}(\{k\})$. Because all bare quantities and fields are independent of μ , $\mu \frac{d}{d\mu} G_B^{(n_\psi, n_a)}(\{k_B\}) = 0$, which leads to a Callan-Symanzik equation for the renormalized correlation function:

$$\left[\mu \frac{\partial}{\partial \mu} + b_\alpha \alpha \frac{\partial}{\partial \alpha} + \gamma_z k_\tau \frac{\partial}{\partial k_\tau} + \frac{n_\psi \gamma_\psi}{2} + (n_a - 1) \gamma_z \right] G^{(n_\psi, n_a)} = 0 \quad (6)$$

with

$$b_\alpha \equiv \frac{\mu}{\alpha} \frac{d\alpha}{d\mu} = -\frac{\mu}{Z_\alpha} \frac{dZ_\alpha}{d\mu}, \quad \gamma_z \equiv -\frac{\mu}{Z_\tau} \frac{dZ_\tau}{d\mu}, \quad \gamma_\psi \equiv \frac{\mu}{Z_\psi} \frac{dZ_\psi}{d\mu}. \quad (7)$$

Note that the beta function of α is $\beta(\alpha) = b_\alpha \alpha$.

On the other hand, suppose the engineering dimension of $G^{(n_\psi, n_a)}$ is Δ_0 . By dimensional analysis, it must have the form $G^{(n_\psi, n_a)} = \mu^{\Delta_0} g\left(\frac{\{k_\tau\}}{\mu^2}, \frac{\{k_x\}}{\mu^2}, \frac{\{k_y\}}{\mu}, \alpha, \frac{\Lambda_y}{\mu}\right)$, where g is some function. Thus,

$$\left(\mu \frac{\partial}{\partial \mu} + 2k_\tau \frac{\partial}{\partial k_\tau} + 2k_x \frac{\partial}{\partial k_x} + k_y \frac{\partial}{\partial k_y} + \Lambda_y \frac{\partial}{\partial \Lambda_y} - \Delta_0 \right) G^{(n_\psi, n_a)} = 0. \quad (8)$$

Combining this equation with Eq. (6) yields another form of the Callan-Symanzik equation:

$$\left[(2 - \gamma_z) k_\tau \frac{\partial}{\partial k_\tau} + 2k_x \frac{\partial}{\partial k_x} + k_y \frac{\partial}{\partial k_y} + \Lambda_y \frac{\partial}{\partial \Lambda_y} - b_\alpha \alpha \frac{\partial}{\partial \alpha} - \Delta_0 - \frac{n_\psi \gamma_\psi}{2} - (n_a - 1) \gamma_z \right] G^{(n_\psi, n_a)} = 0. \quad (9)$$

At the fixed point, $b_\alpha = 0$, and the above equation implies the following scaling structure of the correlation function

$$G^{(n_\psi, n_a)}(s^z \{k_\tau\}, s^2 \{k_x\}, s \{k_y\}, s \Lambda_y) = s^{\Delta} G^{(n_\psi, n_a)}(\{k_\tau\}, \{k_x\}, \{k_y\}, \Lambda_y) \quad (10)$$

with $z \equiv 2 - \gamma_z$ the dynamical exponent, and $\Delta \equiv \Delta_0 + \frac{n_\psi \gamma_\psi}{2} + (n_a - 1)\gamma_z$ the total scaling dimension of this correlation function. It is clear that γ_ψ and $2\gamma_z$ can be interpreted as the anomalous dimensions of the fermionic and gauge fields, respectively. Note that the anomalous dimension of the gauge field $a(k)$ is entirely from a rescaling of time (by setting $k_{\tau B} = Z_\tau k_\tau$), while its real-space counterpart $a(x)$ has no anomalous dimension due to the Ward identity. Also note that the renormalized correlation function would not depend on Λ_y in the absence of any UV/IR mixing, but one of the central results of this paper is that there is UV/IR mixing.

Before finishing this section, we describe an equivalent way to analyze the theory, which is also often used in the literature and differs from the above one by some convention [1–6]. We will mainly use the previous convention, and readers not interested in this part can skip it. In the alternative convention, the bare action is written as

$$\begin{aligned} S_\psi &= \int [dk] \sum_{i,p} \psi_{ip}^\dagger(k) (-iZ_f Z_\eta \eta k_\tau + Z_f(p k_x + k_y^2)) \psi_{ip}(k), \\ S_{\text{int}} &= \int [dk_1][dk_2] \sum_{i,p} Z_f \lambda_p a(-k_1) \psi_{ip}^\dagger(k_2) \psi_{ip}(k_1 + k_2), \\ S_a &= \int [dk] \frac{1}{Z_e} \frac{N}{2e^2 \mu^\epsilon} |k_y|^{1+\epsilon} a(-k) a(k), \end{aligned} \quad (11)$$

and $[dk] = \frac{dk_\tau dk_x dk_y}{(2\pi)^3}$, $\lambda_\pm = \pm 1$. Again, the Ward identity is used to guarantee that the renormalization factor in S_{int} is Z_f , the same as that of the $p k_x + k_y^2$ part of the fermionic kinetic term. The difference between this convention and our previous one is that in this case k_τ has the same dimension as k_x . Instead, another dimensionless parameter η is introduced to keep track of a nontrivial dynamical exponent. Below we will see that, not surprisingly, these two conventions are equivalent. The bare quantities and fields are related to the renormalized ones via

$$(k_{\tau B}, k_{xB}, k_{yB}) = (k_\tau, k_x, k_y), \quad \psi_{ipB} = \sqrt{Z_f} \psi_{ip}, \quad a_B = a, \quad \eta_B = Z_\eta \eta = 1, \quad e_B^2 \equiv Z_e e^2. \quad (12)$$

The engineering dimensions are also given by (4) with the extra $[\eta]_0 = 0$. We also define $\tilde{\alpha} \equiv \frac{\gamma e^2}{\eta}$ with $\gamma = 1/(4\pi)$. Similar to the previous convention, the Z factors are determined by demanding the renormalization conditions given in Eq. (5), but with μ^2 changed to μ^2/η in the first renormalization condition:

$$\frac{\partial \Sigma(k_\tau = \mu^2/\eta, k_x = k_y = 0)}{\partial k_\tau} = 0. \quad (13)$$

Now consider a correlation function involving n_f fermionic fields and n_c gauge fields, denoted by $G^{(n_f, n_c)}$. One can show that $G^{(n_f, n_c)} = \eta^{\frac{n_f}{2} + n_c - 1} \mu^{\Delta_0} g\left(\frac{\eta \{k_\tau\}}{\mu^2}, \frac{\{k_x\}}{\mu^2}, \frac{\{k_y\}}{\mu}, \tilde{\alpha}, \frac{\Lambda_y}{\mu}\right)$, where Δ_0 is the engineering dimension of the correlation function, and g is the same function as in the previous convention. This implies that $\eta \frac{\partial}{\partial \eta} G^{(n_f, n_c)} = \left(\frac{n_f}{2} + n_c - 1 + k_\tau \frac{\partial}{\partial k_\tau} - e^2 \frac{\partial}{\partial e^2}\right) G^{(n_f, n_c)}$. Combining this result and analogous derivations as before, similar Callan-Symanzik equations can be obtained

$$\begin{aligned} &\left(\mu \frac{\partial}{\partial \mu} + b_e e^2 \frac{\partial}{\partial e^2} + b_\eta \eta \frac{\partial}{\partial \eta} + \frac{n_f}{2} \gamma_f\right) G^{(n_f, n_c)} = 0, \\ &\left[\mu \frac{\partial}{\partial \mu} + (b_e - b_\eta) e^2 \frac{\partial}{\partial e^2} + b_\eta k_\tau \frac{\partial}{\partial k_\tau} + \frac{n_f}{2} (\gamma_f + b_\eta) + (n_c - 1) b_\eta\right] G^{(n_f, n_c)} = 0, \\ &\left[(2 - b_\eta) k_\tau \frac{\partial}{\partial k_\tau} + 2k_x \frac{\partial}{\partial k_x} + k_y \frac{\partial}{\partial k_y} + \Lambda_y \frac{\partial}{\partial \Lambda_y} - (b_e - b_\eta) e^2 \frac{\partial}{\partial e^2} - \Delta_0 - \frac{n_f}{2} (\gamma_f + b_\eta) - (n_c - 1) b_\eta\right] G^{(n_f, n_c)} = 0, \end{aligned} \quad (14)$$

where

$$b_\eta \equiv \frac{\mu}{\eta} \frac{d\eta}{d\mu}, \quad b_e \equiv \frac{\mu}{e^2} \frac{de^2}{d\mu}, \quad \gamma_f \equiv \frac{\mu}{Z_f} \frac{dZ_f}{d\mu}. \quad (15)$$

It is not hard to see that b_η , $b_e - b_\eta$ and $\gamma_f + b_\eta$ should be identified as γ_z , b_α and γ_ψ in the previous convention, respectively, and the two conventions ultimately lead to identical results. Note that in this convention, the beta function for $\tilde{\alpha}$ is $\beta(\tilde{\alpha}) = (b_e - b_\eta) \tilde{\alpha}$. In this paper, we will mainly use the previous convention.

II. Summary of the RG Results

The Z factors introduced in Eq. (2) are calculated in Sec. III. Here we summarize the results. We expand Z in powers of $1/N$, and at each order of $1/N$, we keep results relevant to the calculations of b_α , γ_z and γ_ψ to the leading order in Λ_y/μ :

$$\begin{aligned} Z_1 &= 1 - \frac{1}{N} \cdot \frac{2\alpha}{\pi} \ln \frac{\Lambda_y}{\sqrt{\alpha}\mu} + \frac{1}{N^2} \cdot \frac{2\alpha^3}{\pi^2} (S^a(\alpha) + T^a(\alpha) + 2G^a(\alpha) - S^b(\alpha) - T^b(\alpha) - 2G^b(\alpha)) \ln \frac{\Lambda_y}{\mu}, \\ Z_2 &= 1 + \frac{1}{N^2} \cdot \frac{2\alpha^3}{\pi^2} (S^a(\alpha) + T^a(\alpha) - S^b(\alpha) - T^b(\alpha)) \ln \frac{\Lambda_y}{\mu}, \\ Z_3 &\approx 1 - \frac{1}{N} \cdot \frac{2\alpha^3}{\pi} F(\alpha) + \frac{1}{N^2} \cdot \frac{4\alpha^4}{3\pi^2} \left(\ln \frac{\Lambda_y}{\mu} \right)^2, \end{aligned} \quad (16)$$

where the functions $F(\alpha), G^a(\alpha), S^a(\alpha), T^a(\alpha), G^b(\alpha), S^b(\alpha), T^b(\alpha)$ can be found in Eqs. (33), (47), (48), (50), (55), (56), (57), respectively. Using these expressions, Eqs. (3) and (7), b_α , γ_z and γ_ψ are obtained to be

$$\begin{aligned} b_\alpha &\approx \frac{1}{N} \cdot \frac{2\alpha}{\pi} - \frac{1}{N^2} \cdot \frac{8\alpha^4}{3\pi^2} \ln \frac{\Lambda_y}{\mu}, \\ \gamma_z &= -\frac{1}{N} \cdot \frac{2\alpha}{\pi} + \frac{1}{N^2} \cdot \left(\frac{4\alpha^3}{\pi^2} (G^a(\alpha) - G^b(\alpha)) - \frac{2\alpha^2}{\pi^2} \right), \\ \gamma_\psi &= -\frac{1}{N} \cdot \frac{2\alpha}{\pi} + \frac{1}{N^2} \cdot \left(\frac{2\alpha^3}{\pi^2} (2G^a(\alpha) - S^a(\alpha) - T^a(\alpha) - 2G^b(\alpha) + S^b(\alpha) + T^b(\alpha)) - \frac{2\alpha^2}{\pi^2} \right). \end{aligned} \quad (17)$$

Here we ignore $\frac{1}{N^2} \ln \frac{\Lambda_y}{\mu}$ term in Z_3 and keep only terms proportional to $\ln \frac{\Lambda_y}{\mu}$ at order $1/N^2$ in b_α . Note that almost all terms in b_α , γ_z and γ_ψ come from explicit μ dependence in Z except for the $\frac{1}{N^2}\alpha^2$ term, which comes from the $\ln \sqrt{\alpha}$ term in Z_1 .

III. Feynman Diagram Calculations

In this section, we present the details of the Feynman diagram calculations leading to the results summarized in Section II. Parts of the relevant calculations can be found in Refs. [1, 3–5, 7, 8]. Here we focus on the case where $\epsilon = 0$.¹ We will also assume that external k_y to be positive for self-energies unless mentioned otherwise.

First, we collect results of all the Feynman diagrams contributing to the self-energy of boson and fermion to the third leading order in the large- N expansion. We will see that all of the divergent diagrams give the traditional logarithmic divergence except for the Benz diagram and the 3-String diagram, which give the unconventional double logarithmic divergence. In any case, $Z_{1,2,3}$ can be expanded in $1/N$ as

$$Z_i = 1 + \frac{1}{N} \delta_i^{(1)} + \frac{1}{N^2} \delta_i^{(2)} \quad i = 1, 2, 3 \quad (18)$$

such that renormalization conditions Eq. (5) are satisfied. The propagator of a , denoted as $\mathcal{D}(k)$, and the propagator of ψ , denoted as $\mathcal{G}(k)$, to the third leading order in $1/N$ are written as

$$\begin{aligned} \mathcal{D}^{-1} &= ND^{-1} - \Pi^{(1)} - \frac{1}{N} \Pi^{(2)} + \dots \\ \mathcal{G}^{-1} &= G^{-1} - \frac{1}{N} \Sigma^{(1)} - \frac{1}{N^2} \Sigma^{(2)} + \dots, \end{aligned} \quad (19)$$

where D is the leading-order propagator for a as in e.g. Ref. [1]

$$D(k_\tau, k_y) = \frac{1}{\gamma \frac{|k_\tau|}{|k_y|} + \frac{|k_y|}{e^2}} \quad (20)$$

¹ As discussed in Ref. [3], if we use the second convention, we need to set $\eta \sim \mathcal{O}(1)$ such that the large- N expansion has no extra factors of N from η .

with $\gamma = 1/(4\pi)$, and G is the bare fermion propagator,

$$G_{\pm}(k_{\tau}, k_x, k_y) = \frac{1}{-ik_{\tau} \pm k_x + k_y^2}. \quad (21)$$

We can also write down a large- N expansion of b_{α} , γ_z and γ_{ψ} to the order of $1/N^2$,

$$\begin{aligned} b_{\alpha} &= \frac{1}{N} b_{\alpha}^{(1)} + \frac{1}{N^2} b_{\alpha}^{(2)} + \dots \\ \gamma_z &= \frac{1}{N} \gamma_z^{(1)} + \frac{1}{N^2} \gamma_z^{(2)} + \dots \\ \gamma_{\psi} &= \frac{1}{N} \gamma_{\psi}^{(1)} + \frac{1}{N^2} \gamma_{\psi}^{(2)} + \dots \end{aligned} \quad (22)$$

which can be calculated through solving the Callan-Symanzik equation Eq. (6) from the propagator \mathcal{D}, \mathcal{G} at the third leading order of $1/N$, or through Eq. (7).

A. Second Leading Order Result of Self-Energy

The second leading order result of the fermion self-energy is given by the standard one-loop diagram shown in Fig. 1. The diagram has been computed in [4, 5]. Here we write down the result of the diagram at $\epsilon = 0$ with

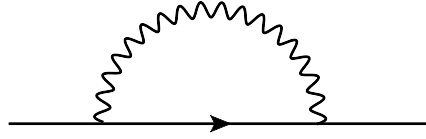


FIG. 1: One-loop diagram for fermion self-energy.

y -momentum cutoff Λ_y ,

$$\Sigma_{1LF}(k) = \int [dl] G_f(k-l)D(l) = ik_{\tau} \frac{e^2}{2\pi^2} \left(\frac{1}{2} + \ln \left(\frac{\Lambda_y}{\sqrt{\gamma e^2 |k_{\tau}|}} \right) \right). \quad (23)$$

To impose the renormalization conditions in Eq. (5), we take

$$\delta_1^{(1)} = -\frac{2\alpha}{\pi} \ln \left(\frac{\Lambda_y}{\mu\sqrt{\alpha}} \right), \quad \delta_2^{(1)} = 0 \quad (24)$$

with $\alpha \equiv e^2/(4\pi)$.²

Let us then turn to the second leading order result of the self-energy of boson, $\Pi^{(1)}$. At this order only the so-called Aslamazov-Larkin (AL) diagram [9] in Fig. 2 gives non-zero but finite contribution as argued in Ref. [4]. The AL diagram reads [1]

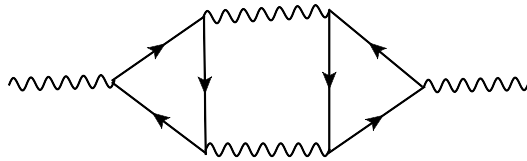


FIG. 2: Aslamazov-Larkin (AL) diagram for boson self-energy.

$$\Pi_{AL}(k) = \frac{1}{2} \int \frac{dl_{\tau} dl_x dl_y}{(2\pi)^3} \Gamma^3(k, l, -(k+l)) \Gamma^3(-k, -l, k+l) D(l) D(k+l) \quad (25)$$

² We note that in the simple minimal subtraction scheme, one would take $\delta^{(1)} = -\frac{2\alpha}{\pi} \ln \frac{\Lambda_y}{\mu}$, which amounts to imposing a different RG condition.

where Γ^3 is the fermion-induced three-boson vertex and receives contributions from both fermion patches as well as both directions in which fermions can travel in the loop,

$$\Gamma^3 = \Gamma_+^3 + \Gamma_-^3, \quad (26)$$

$$\Gamma_s^3(l_1, l_2, -(l_1 + l_2)) = \lambda_s^3 (f_s(l_1, l_2, -(l_1 + l_2)) + f_s(l_2, l_1, -(l_1 + l_2))), \quad (27)$$

$$f_s(l_1, l_2, -(l_1 + l_2)) = - \int \frac{dp_\tau dp_x dp_y}{(2\pi)^3} G_s(p) G_s(p - l_1) G_s(p + l_2). \quad (28)$$

First let us compute $f_\pm(k, l, -(k + l))$. We perform the integral in the sequence of p_x , p_y and p_τ to obtain

$$f_\pm(k, l, -(k + l)) = \frac{1}{4\pi (k_y(il_\tau \mp l_x - l_y^2) - l_y(ik_\tau \mp k_x + k_y^2))} \times \left(k_\tau \theta\left(\frac{k_\tau}{k_y}\right) + l_\tau \theta\left(\frac{l_\tau}{l_y}\right) - (k + l)_\tau \theta\left(\frac{(k + l)_\tau}{(k + l)_y}\right) \right). \quad (29)$$

Here $\theta(x)$ is the unit step function. An important property is that if we take the static limit $k_\tau \rightarrow 0$, the fermion-induced three-boson vertex is non-zero only when the internal boson satisfies,

$$-k_y < l_y < 0, \quad \text{when } k_y > 0 \quad \text{or} \quad 0 < l_y < -k_y, \quad \text{when } k_y < 0, \quad (30)$$

i.e. the integration of the internal boson momentum only has nonzero contribution from a restricted finite region in the static limit.³ Note that the imaginary part of the pole of l_x for both $f_s(k, l, -(k + l))$ and $f_s(l, k, -(k + l))$ with a fixed $s = \pm$ are at $s(l_\tau - k_\tau l_y/k_y)$. Considering the integration of l_x in Eq. (25), we see that Π_{AL} is non-zero only when the two fermion loops come from different patches. After the integration of l_x , we see that the k_x dependence drops out and we have

$$\Pi_{AL}(k_\tau, k_y) = -\frac{1}{64\pi^4 k_y^2} \int dl_\tau dl_y D(l) D(k + l) \left(k_\tau \theta\left(\frac{k_\tau}{k_y}\right) + l_\tau \theta\left(\frac{l_\tau}{l_y}\right) - (k + l)_\tau \theta\left(\frac{(k + l)_\tau}{(k + l)_y}\right) \right)^2 \times \frac{(l_y^2 + k_y l_y)^2}{|l_\tau - k_\tau l_y/k_y| \left((l_\tau - k_\tau l_y/k_y)^2 + (l_y^2 + k_y l_y)^2 \right)}. \quad (31)$$

It is straightforward to see that this integral is convergent from the kinematic constraint in Eq. (30). Here, we focus on $\Pi_{AL}(k_\tau = 0, k_y)$. Also we temporarily assume $k_y > 0$, which indicates that $-k_y < l_y < 0$. After a change of variable with $l_\tau = k_y^2 \Delta$ ($-\infty < \Delta < \infty$) and $l_y = k_y \delta$ ($-1 < \delta < 0$), the final result is given as follows,

$$\Pi_{AL}(k_\tau = 0, k_y) = -\frac{|k_y| 2\alpha^3}{e^2 \pi} F(\alpha), \quad (32)$$

where

$$F(\alpha) \equiv \int_0^1 d\delta \int_0^\infty d\Delta \frac{\delta}{\delta^2 + \alpha\Delta} \frac{1 - \delta}{(1 - \delta)^2 + \alpha\Delta} \frac{\Delta (\delta^2 - \delta)^2}{\Delta^2 + (\delta^2 - \delta)^2}. \quad (33)$$

To impose the renormalization conditions in Eq. (5), we take the counterterm to be

$$\delta_3^{(1)} = -\frac{2\alpha^3}{\pi} F(\alpha) \quad (34)$$

³ This is the reason why we do not see the double log divergence in lower order diagrams. In $U(1) \times U(1)$ or $U(2)$ gauge theory [5], this also leads to the fact that there is a fixed line instead of several isolated fixed points at the leading order of the RG equation. It is straightforward to see that the fixed line will in principle be lifted because of the third leading order results of (boson) self-energy.

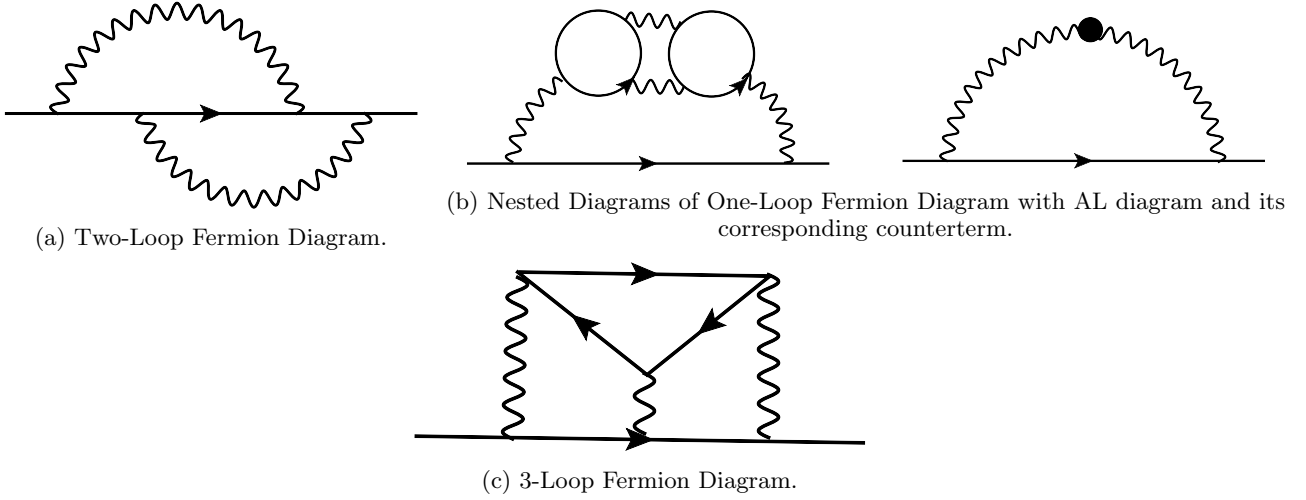


FIG. 3: Diagrams contributing to the third leading order of fermion self-energy.

B. Third Leading Order Result of Fermion Self-Energy

Next, we move to the self-energies at the third leading order of $1/N$. Because the goal is to compute the beta functions to the order of $1/N^2$, it is sufficient to keep only the divergent parts in the self-energies. We start from the fermion self-energy. There are four non-zero diagrams as shown in Fig. 3. The two-loop fermion diagram in Fig. 3a is convergent, while the divergence of the two nested diagrams shown in Fig. 3b cancel with each other. Thus, the divergent part only comes from the three-loop diagram, shown in Fig. 3c.

In the three-loop diagram, the fermion in the top loop can run in the clockwise or counterclockwise direction. Moreover, only when the fermion running in the loop lies in a different \pm patch than the external fermion [1, 10] will the diagram give logarithmic divergence. Let us assume that the external fermion lies in the $+$ patch. First, consider the case in which the fermion in the loop travels in counterclockwise direction. Its contribution reads

$$\Sigma_{3LF}^a(k) = -\lambda_+^3 \lambda_-^3 \int \frac{[dl_1][dl_2][dp]}{(2\pi)^9} G_+(k-l_1)G_+(k-l_2)G_-(p)G_-(p+l_1)G_-(p+l_2) \times D(l_1)D(l_1-l_2)D(l_2). \quad (35)$$

Integrating over l_{1x}, l_{2x} results in

$$\Sigma_{3LF}^a(k) = - \int \frac{dp_\tau dp_x dp_y dl_{1\tau} dl_{1y} dl_{2\tau} dl_{2y}}{(2\pi)^7} \frac{\theta(l_{1\tau} - k_\tau) - \theta(-l_{1\tau} - p_\tau)}{i(k_\tau - p_\tau - 2l_{1\tau}) + 2(k_y + p_y)l_{1y} - p_x + p_y^2 - k_x - k_y^2} \times \frac{\theta(l_{2\tau} - k_\tau) - \theta(-l_{2\tau} - p_\tau)}{i(k_\tau - p_\tau - 2l_{2\tau}) + 2(k_y + p_y)l_{2y} - p_x + p_y^2 - k_x - k_y^2} \cdot \frac{1}{-ip_\tau - p_x + p_y^2} D(l_1)D(l_1-l_2)D(l_2). \quad (36)$$

Integrating over p_x and p_y , we obtain

$$\Sigma_{3LF}^a(k) = \int \frac{dp_\tau dl_{1\tau} dl_{1y} dl_{2\tau} dl_{2y}}{(2\pi)^5} \frac{D(l_1)D(l_1-l_2)D(l_2)}{2((l_2-l_1)_y G_+(k)^{-1} + 2i(l_{2y}l_{1\tau} - l_{1y}l_{2\tau}))} T(p_\tau; l_{1\tau}, l_{2\tau}; l_{1y}, l_{2y}; k_\tau), \quad (37)$$

where $G_+(k)^{-1}$ is just the inverse of bare $+$ patch fermion propagator and

$$T(p_\tau; l_{1\tau}, l_{2\tau}; l_{1y}, l_{2y}; k_\tau) = (\theta(l_{1\tau} - k_\tau) - \theta(-l_{1\tau} - p_\tau)) (\theta(l_{2\tau} - k_\tau) - \theta(-l_{2\tau} - p_\tau)) \times \left[\left(\theta\left(\frac{2l_{2\tau} - k_\tau}{l_{2y}}\right) - \theta\left(\frac{2l_{1\tau} - k_\tau}{l_{1y}}\right) \right) \theta(-p_\tau) + \left(\theta\left(\frac{2l_{1\tau} - k_\tau}{l_{1y}}\right) - \theta\left(\frac{l_{2\tau} - l_{1\tau}}{l_{2y} - l_{1y}}\right) \right) \theta(k_\tau - p_\tau - 2l_{1\tau}) - \left(\theta\left(\frac{2l_{2\tau} - k_\tau}{l_{2y}}\right) - \theta\left(\frac{l_{2\tau} - l_{1\tau}}{l_{2y} - l_{1y}}\right) \right) \theta(k_\tau - p_\tau - 2l_{2\tau}) \right]. \quad (38)$$

Suppose $k_\tau > 0$. Separating l_{1y}, l_{2y} plane into six regions as in Fig. 4a and doing the integration of p_τ , we obtain

$$\mathcal{T}(l_{1\tau}, l_{2\tau}; l_{1y}, l_{2y}; k_\tau) \equiv \int dp_\tau T(p_\tau; l_{1\tau}, l_{2\tau}; l_{1y}, l_{2y}; k_\tau) \quad (39)$$

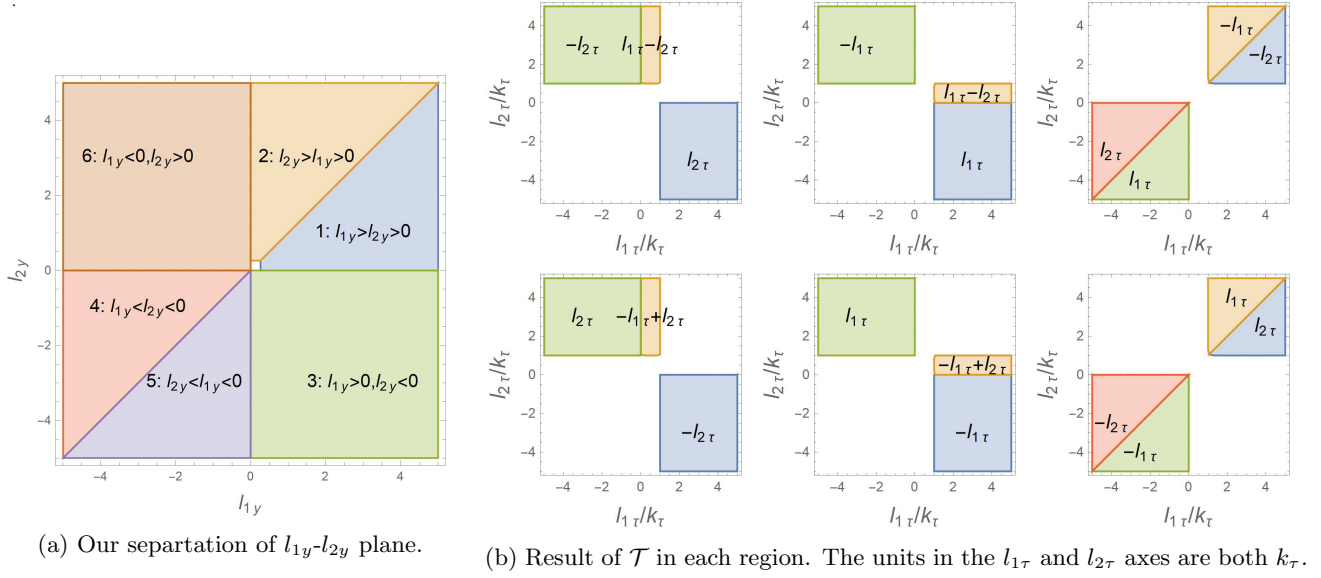


FIG. 4: Result of \mathcal{T} given different sections on the $l_{1y} - l_{2y}$ plane. Different sections of $l_{1y} - l_{2y}$ plane are labeled in Fig. 4a and the result of \mathcal{T} in each region is given in Fig. 4b where each graph from left to right then from top down corresponds to the result in section 1-6 respectively.

in each region shown in Fig. 4b (k_τ is set to be 1 in these graphs).

Note that

$$\mathcal{T}(l_{1\tau}, l_{2\tau}; -l_{1y}, -l_{2y}; k_\tau) = -\mathcal{T}(l_{1\tau}, l_{2\tau}; l_{1y}, l_{2y}; k_\tau) \quad (40)$$

and therefore regions connected by $l_{1y}, l_{2y} \iff -l_{1y}, -l_{2y}$ gives the same result. We can thus restrict to regions with $l_{1y} > 0$. First consider region 1. In order to isolate the divergent terms, let us do the following change of parameters:

$$l_{2y} = l_{1y}\delta, \quad l_{1\tau} = l_{1y}^2\Delta_1, \quad l_{2\tau} = l_{1y}^2\Delta_2, \quad k_\tau = l_{1y}^2\Delta_0. \quad (41)$$

Moreover, we can write down \mathcal{T} as

$$\mathcal{T}(l_{2\tau}, l_{1\tau}; l_{2y}, l_{1y}; k_\tau) = l_{1y}^2 \mathcal{T}_0(\Delta_1, \Delta_2; \delta; \Delta_0). \quad (42)$$

Then we have

$$\begin{aligned} \Sigma_{3LF}^a(k) &= \frac{i\alpha^3}{2\pi^2} \int dl_{1y} d\delta d\Delta_1 d\Delta_2 \frac{l_{1y}}{(\Delta_2 - \delta\Delta_1) - \frac{1}{2}i(1-\delta)\frac{G_+(k)^{-1}}{l_{1y}^2}} \mathcal{T}_0 \\ &\times \frac{1}{1 + \alpha|\Delta_1|} \frac{|\delta|}{|\delta|^2 + \alpha|\Delta_2|} \frac{|1-\delta|}{|1-\delta|^2 + \alpha|\Delta_1 - \Delta_2|}. \end{aligned} \quad (43)$$

The divergent terms come from the integration region $l_{1y} \rightarrow \infty$, so let us do the integration of l_{1y} from k_y , the dynamically generated IR cutoff, to infinity instead. We can thus first do a large l_{1y} expansion in this region,

$$\Sigma_{3LF}^a(k) = \frac{i\alpha^3}{2\pi^2} \left(\sigma_1 \int l_{1y} dl_{1y} + i\sigma_2 G_+(k)^{-1} \int l_{1y}^{-1} dl_{1y} + \sigma_3 k_\tau \int l_{1y}^{-1} dl_{1y} + \dots \right), \quad (44)$$

where

$$\begin{aligned} \sigma_1 &= \int d\delta d\Delta_1 d\Delta_2 \frac{1}{\Delta_2 - \delta\Delta_1} \frac{1}{1 + \alpha|\Delta_1|} \frac{|\delta|}{|\delta|^2 + \alpha|\Delta_2|} \frac{|1-\delta|}{|1-\delta|^2 + \alpha|\Delta_1 - \Delta_2|} \mathcal{T}_0(\Delta_1, \Delta_2; \delta; 0), \\ \sigma_2 &= \int d\delta d\Delta_1 d\Delta_2 \frac{1-\delta}{2(\Delta_2 - \delta\Delta_1)^2} \frac{1}{1 + \alpha|\Delta_1|} \frac{|\delta|}{|\delta|^2 + \alpha|\Delta_2|} \frac{|1-\delta|}{|1-\delta|^2 + \alpha|\Delta_1 - \Delta_2|} \mathcal{T}_0(\Delta_1, \Delta_2; \delta; 0), \\ \sigma_3 &= \frac{d}{d\Delta_0} \left(\int d\delta d\Delta_1 d\Delta_2 \frac{1}{\Delta_2 - \delta\Delta_1} \frac{1}{1 + \alpha|\Delta_1|} \frac{|\delta|}{|\delta|^2 + \alpha|\Delta_2|} \frac{|1-\delta|}{|1-\delta|^2 + \alpha|\Delta_1 - \Delta_2|} \mathcal{T}_0(\Delta_1, \Delta_2; \delta; \Delta_0) \right) \Big|_{\Delta_0=0}. \end{aligned} \quad (45)$$

The integration of the ... terms is convergent. The term proportional to σ_1 is polynomially divergent and does not contribute to the logarithmic divergence, so it should give an unimportant shift of chemical potential. The term proportional to σ_2 and σ_3 give the following logarithmically divergent contribution to $\Sigma_{3LF}^a(k)$:

$$\left(\frac{\alpha^3}{2\pi^2} S^a(\alpha) G_+(k)^{-1} - \frac{\alpha^3}{\pi^2} G^a(\alpha) i k_\tau \right) \ln \left(\frac{\Lambda_y}{k_y} \right), \quad (46)$$

where $G^a(\alpha)$ and $S^a(\alpha)$ are defined as follows

$$G^a(\alpha) \equiv \int_0^1 d\delta \int_0^\infty d\Delta \frac{\delta}{\delta^2 + \alpha\Delta} \frac{1 - \delta}{(1 - \delta)^2 + \alpha\Delta}, \quad (47)$$

$$S^a(\alpha) \equiv \int_0^1 d\delta \int_0^\infty d\Delta_1 \int_0^\infty d\Delta_2 \frac{(1 - \delta)\Delta_2}{(\Delta_2 + \delta\Delta_1)^2} \frac{1}{1 + \alpha\Delta_1} \frac{\delta}{\delta^2 + \alpha\Delta_2} \frac{1 - \delta}{(1 - \delta)^2 + \alpha(\Delta_1 + \Delta_2)}. \quad (48)$$

The calculation in the region 2 is completely analogous to the calculation in the region 1. If 1 and 2 are exchanged in Eqs. (37) and (38), one can see that the result in region 2 is identical to the result in region 1. For region 3, it is clear that $\sigma_3 = 0$ while from σ_2 we obtain the divergent part

$$\frac{\alpha^3}{\pi^2} G_+(k)^{-1} T^a(\alpha) \ln \left(\frac{\Lambda_y}{k_y} \right), \quad (49)$$

where

$$T^a(\alpha) \equiv \int_0^\infty d\delta \int_0^\infty d\Delta_1 \int_0^{\Delta_1} d\Delta_2 \frac{(1 + \delta)\Delta_2}{(\Delta_2 + \delta\Delta_1)^2} \frac{1}{1 + \alpha\Delta_1} \frac{\delta}{\delta^2 + \alpha\Delta_2} \frac{1 + \delta}{(1 + \delta)^2 + \alpha(\Delta_1 - \Delta_2)}. \quad (50)$$

Adding the results of all regions up, we get the result for the case in which the fermion travels in counterclockwise direction:

$$\Sigma_{3LF}^a(k) \rightarrow \frac{2\alpha^3}{\pi^2} (S^a(\alpha) + T^a(\alpha)) G_+(k)^{-1} \ln \left(\frac{\Lambda_y}{k_y} \right) - \frac{4\alpha^3}{\pi^2} G^a(\alpha) i k_\tau \ln \left(\frac{\Lambda_y}{k_y} \right). \quad (51)$$

The calculation of the case in which the fermion travels clockwise is completely analogous with similar expressions. The diagram reads

$$\begin{aligned} \Sigma_{3LF}^b(k) = & -\lambda_+^3 \lambda_-^3 \int \frac{[dl_1][dl_2][dp]}{(2\pi)^9} G_+(k - l_1) G_+(k - l_2) G_-(p) G_-(p - l_1) G_-(p - l_2) \\ & \times D(l_1) D(l_1 - l_2) D(l_2). \end{aligned} \quad (52)$$

Integrate over l_{1x} , l_{2x} , p_x and p_y in order, we have

$$\Sigma_{3LF}^b(k) = - \int \frac{dp_\tau dl_{1\tau} dl_{1y} dl_{2\tau} dl_{2y}}{(2\pi)^5} \frac{D(l_1) D(l_1 - l_2) D(l_2)}{2[(l_2 - l_1)_y G_+(k)^{-1} + 2i(l_{2y} l_{1\tau} - l_{1y} l_{2\tau} - i(l_{1y}^2 l_{2y} - l_{1y} l_{2y}^2))]} T(p_\tau; l_{1\tau}, l_{2\tau}; l_{1y}, l_{2y}; k_\tau), \quad (53)$$

where $T(p_\tau; l_{1\tau}, l_{2\tau}; l_{1y}, l_{2y}; k_\tau)$ is precisely the same as what was defined in Eq. (38). Following closely the procedure outlined, we have

$$\Sigma_{3LF}^b(k) \rightarrow - \frac{2\alpha^3}{\pi^2} (S^b(\alpha) + T^b(\alpha)) G_+(k)^{-1} \ln \left(\frac{\Lambda_y}{k_y} \right) + \frac{4\alpha^3}{\pi^2} G^b(\alpha) i k_\tau \ln \left(\frac{\Lambda_y}{k_y} \right), \quad (54)$$

where $G^b(\alpha)$ is defined as

$$G^b(\alpha) \equiv \int_0^1 d\delta \int_0^\infty d\Delta \frac{\delta}{\delta^2 + \alpha\Delta} \frac{1 - \delta}{(1 - \delta)^2 + \alpha\Delta} \frac{\Delta^2}{\Delta^2 + (\delta^2 - \delta)^2}, \quad (55)$$

and $S^b(\alpha)$ and $T^b(\alpha)$ are defined as

$$\begin{aligned} S^b(\alpha) \equiv & \int_0^1 d\delta \int_0^\infty d\Delta_1 \int_0^\infty d\Delta_2 \frac{(1 - \delta)\Delta_2 ((\Delta_2 + \delta\Delta_1)^2 - (\delta^2 - \delta)^2)}{((\Delta_2 + \delta\Delta_1)^2 + (\delta - \delta^2)^2)^2} \\ & \times \frac{1}{1 + \alpha\Delta_1} \frac{\delta}{\delta^2 + \alpha\Delta_2} \frac{1 - \delta}{(1 - \delta)^2 + \alpha(\Delta_1 + \Delta_2)}, \end{aligned} \quad (56)$$

$$T^b(\alpha) \equiv \int_0^\infty d\delta \int_0^\infty d\Delta_1 \int_0^{\Delta_1} d\Delta_2 \frac{(1+\delta)\Delta_2 ((\Delta_2 + \delta\Delta_1)^2 - (\delta^2 + \delta)^2)}{((\Delta_2 + \delta\Delta_1)^2 + (\delta^2 + \delta)^2)^2} \times \frac{1}{1 + \alpha\Delta_1} \frac{\delta}{\delta^2 + \alpha\Delta_2} \frac{1 + \delta}{(1 + \delta)^2 + \alpha(\Delta_1 - \Delta_2)}. \quad (57)$$

Collecting the results for fermion self-energy at this order, we obtain the counter terms:

$$\begin{aligned} \delta_1^{(2)} &= \frac{2\alpha^3}{\pi^2} (S^a(\alpha) + T^a(\alpha) + 2G^a(\alpha) - S^b(\alpha) - T^b(\alpha) - 2G^b(\alpha)) \ln \frac{\Lambda_y}{\mu} \\ \delta_2^{(2)} &= \frac{2\alpha^3}{\pi^2} (S^a(\alpha) + T^a(\alpha) - S^b(\alpha) - T^b(\alpha)) \ln \frac{\Lambda_y}{\mu} \end{aligned} \quad (58)$$

where $G^a(\alpha), S^a(\alpha), T^a(\alpha), G^b(\alpha), S^b(\alpha), T^b(\alpha)$ are defined in Eqs. (47), (48), (50), (55), (56), (57) respectively.

Before we continue, let us mention that from the Ward identity [1], the fermion field strength divergence is the same as the divergence of fermion-gauge vertex, whose contribution to order $1/N^2$ comes solely from Fig. 5 [8].

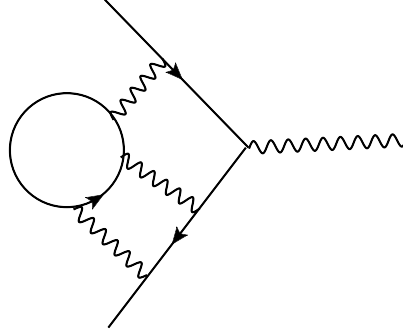


FIG. 5: Diagram contributing to the divergence of fermion-fermion-boson vertex at order $1/N^2$.

C. Third leading Order Result of Boson Self-Energy

In this subsection, we evaluate the boson self energy at the third leading order and calculate $\delta_3^{(2)}$, the contribution to Z_3 at the order of $1/N^2$. Again, it is sufficient to keep only the divergent parts. It turns out that $\delta_3^{(2)}$ is double-logarithmic (double-log) divergent, i.e., $\delta_3^{(2)} \propto \left(\ln \frac{\Lambda_y}{\mu}\right)^2$, with μ the renormalization scale. The leading contribution in the limit of $\mu \ll \Lambda_y$ is

$$\delta_3^{(2)} = \frac{4\alpha^4}{3\pi^2} \left(\ln \frac{\Lambda_y}{\mu}\right)^2 \quad (59)$$

This result can be obtained by combining Eqs. (93), (114) and the renormalization condition in Eq. (5). The rest of this subsection is devoted to the computational details.

1. General Strategies of Calculation and Assumptions

Since the higher-loop diagrams are much more difficult to compute explicitly, we begin by outlining the general strategies we use and spell out assumptions we make to simplify our calculations.

We draw all diagrams contributing to the third leading order, i.e. order $1/N$, of boson self-energy (see Fig. 6). It turns out that some diagrams have internal boson momenta restricted as in Eq. (30). Using the calculation of the AL diagram and the results in quantum field theory (QFT), we make the following *local divergence* assumption: *integration with restricted y-momentum is convergent when the Feynman diagram contains no divergent subdiagrams*. Hence, only two sets of diagrams can contribute to double-log divergence, which we call Benz diagram and 3-String diagram, and denote the results of these two sets of diagrams by $\Pi_{\text{Benz}}(k_y)$ and $\Pi_{\text{3String}}(k_y)$, respectively.

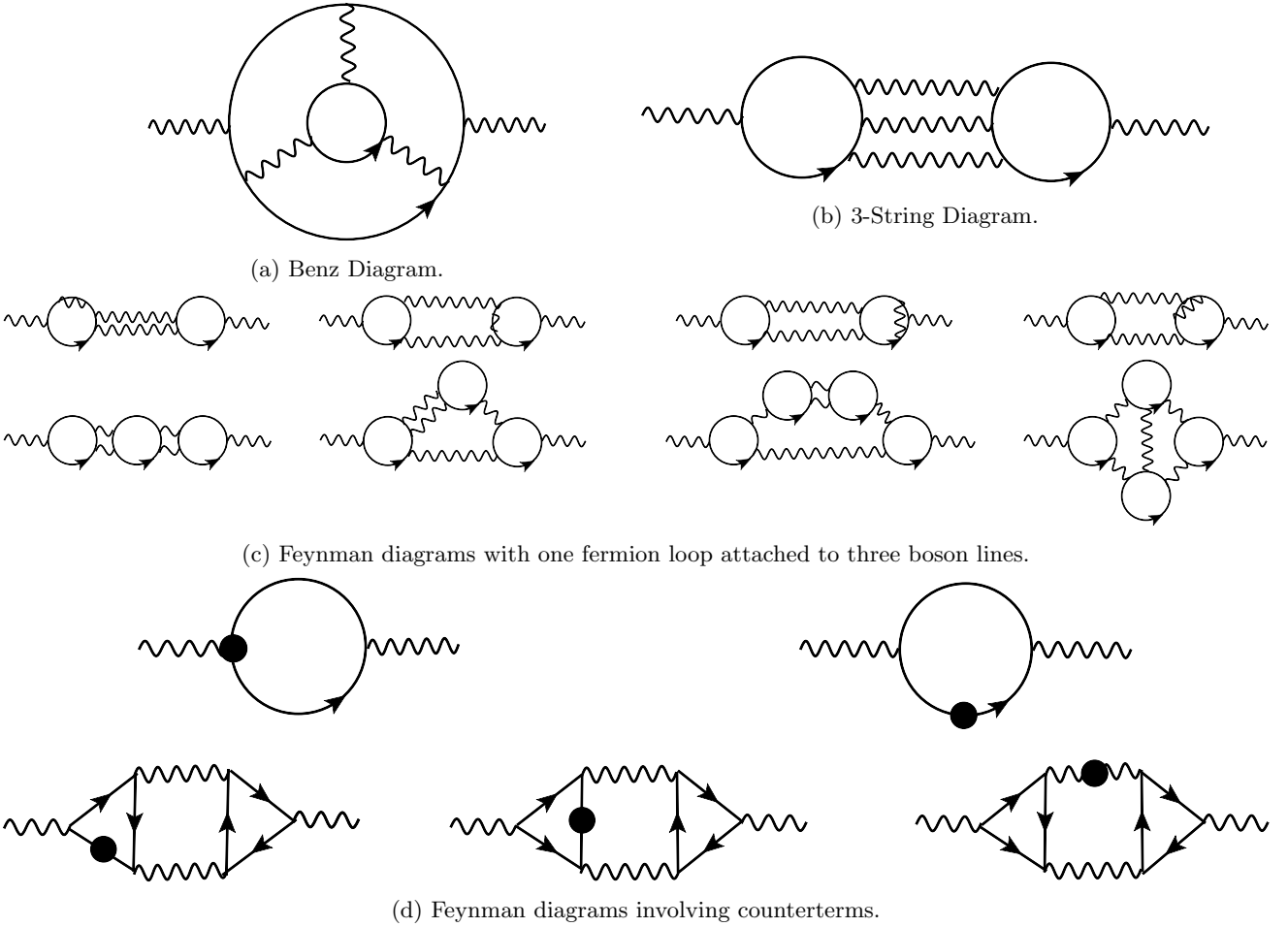


FIG. 6: Diagrams contributing to the third leading order of boson self-energy. We do not repeat all the possible reshuffling of boson lines when attached to a fermion loop. We also do not include Feynman diagrams with only one fermion loop, which are deemed to be zero in the static limit $k_\tau \rightarrow 0$ [1, 3].

For these two sets of diagrams, we can first use the residue theorem to integrate the x -momentum of all internal propagators, as well as frequency and y -momentum of the two fermion loops. Then we are left with the integration of internal boson frequency and y -momentum, denoted as $l_{i\tau}$ and l_{iy} , with $i = 1, 2$ for two internal boson lines. It turns out that at $k_\tau = 0$ these two contributions to the self energy take the form of $\Pi_{\text{Benz}}(k_y) = \frac{1}{|k_y|} \int dl_{1\tau} dl_{1y} dl_{2\tau} dl_{2y} \mathbf{B}(k_y, l_{1\tau}, l_{1y}, l_{2\tau}, l_{2y})$ and $\Pi_{\text{3String}}(k_y) = \frac{1}{|k_y|} \int dl_{1\tau} dl_{1y} dl_{2\tau} dl_{2y} \mathbf{S}(k_y, l_{1\tau}, l_{1y}, l_{2\tau}, l_{2y})$, where \mathbf{B} and \mathbf{S} can be written as

$$\begin{aligned} \mathbf{B}(k_y, l_{1\tau}, l_{1y}, l_{2\tau}, l_{2y}) &= \mathbf{B}(0, l_{1\tau}, l_{1y}, l_{2\tau}, l_{2y}) + a_B(l_{1\tau}, l_{1y}, l_{2\tau}, l_{2y}) \cdot k_y + f_B(k_y, l_{1\tau}, l_{1y}, l_{2\tau}, l_{2y}) \cdot k_y^2, \\ \mathbf{S}(k_y, l_{1\tau}, l_{1y}, l_{2\tau}, l_{2y}) &= \mathbf{S}(0, l_{1\tau}, l_{1y}, l_{2\tau}, l_{2y}) + a_S(l_{1\tau}, l_{1y}, l_{2\tau}, l_{2y}) \cdot k_y + f_S(k_y, l_{1\tau}, l_{1y}, l_{2\tau}, l_{2y}) \cdot k_y^2, \end{aligned} \quad (60)$$

where $a_{B,S}$ is the coefficient of the k_y -term in the Taylor expansion of $\mathbf{B}, \mathbf{S}(k_y, l_{1\tau}, l_{1y}, l_{2\tau}, l_{2y})$, and $f_{B,S}(k_y, l_{1\tau}, l_{1y}, l_{2\tau}, l_{2y})$ are some analytic functions of k_y defined by the above equations. It turns out that the integrations of both $\mathbf{B}(0, l_{1\tau}, l_{1y}, l_{2\tau}, l_{2y})$ and $\mathbf{S}(0, l_{1\tau}, l_{1y}, l_{2\tau}, l_{2y})$ are polynomially divergent for the individual diagrams. In the end, they are canceled among all diagrams related to each other by rearranging the order in which photon lines attach to the fermion loops, e.g. between the Benz diagram in Fig. 6a and its twin diagram in Fig. 7, and among the six cases of 3-String diagrams shown in Fig. 8 [7]. Furthermore, $\Pi(k)$ is an even function of k_y due to the inversion symmetry of the system, so the second terms (i.e., the terms proportional to k_y) in the above equations do not contribute. Hence we just need to integrate $f_{B,S}(k_y, l_{1\tau}, l_{1y}, l_{2\tau}, l_{2y})$, with a cutoff Λ_y for l_{1y} and l_{2y} .

To extract potential double-log divergence in a simpler way, we apply the following *expansion trick* similar to the calculation of fermion self-energy. Since we are interested in the divergent part of the integration as $\Lambda_y \rightarrow \infty$, it is enough to consider the region with sufficiently large l_{iy} and $l_{i\tau}$. Therefore, we can simply integrate $f(k_y, l_{1\tau}, l_{1y}, l_{2\tau}, l_{2y})$ at $k_y = 0$ here, and impose suitable *dynamically generated IR cutoff* for the integrals, i.e.,

the scale above which $f(0, l_{1\tau}, l_{1y}, l_{2\tau}, l_{2y})$ is comparable with $f(k_y, l_{1\tau}, l_{1y}, l_{2\tau}, l_{2y})$. In this way, the coefficient of the double-log divergent term can be extracted. To check the validity of this strategy, we compute the Benz diagram in Sec. III C 3 explicitly and confirm that it gives the same answer as the one obtained from the method explained above.

2. All Diagrams at the Third Leading Order

All diagrams contributing to the boson self-energy to the third leading order in $1/N$ are listed in Fig. 6. For brevity, we do not repeat diagrams related to the ones listed through rearranging the order in which boson lines are attached to a fermion loop. These diagrams are related to each other by the fact that their summation vanishes when external momentum vanishes [7]. Moreover, since we are mostly concerned with divergence in front of the term $|k_y|$ of boson self-energy, we do not include Feynman diagrams which have only one fermion loop because they vanish in the static limit $k_\tau \rightarrow 0$ [1, 3].

Because of the kinetic constraint mentioned in the calculation of AL diagram in (30) [8], at the static limit $k_\tau = 0$, at least one boson's y -momentum in Fig. 6c is bounded by external boson y -momentum k_y . Hence, we conjecture that diagrams in Fig. 6c with no divergent subdiagrams are convergent. In fact, the first two diagrams have divergent subdiagrams corresponding to one-loop fermion self-energy diagram as in Fig. 1, whose divergence is cancelled by the third and fourth diagrams in Fig. 6d involving counterterms.⁴ We conjecture that the rest six diagrams are simply finite like the AL diagram. The first and second diagram in Fig. 6d only give divergence to the Landau damping term, i.e., divergence in the term $|k_\tau|/|k_y|$, and cancel with each other due to the Ward identity. The fifth diagram in Fig. 6d is convergent.

Finally, the Benz diagram as in Fig. 6a is explicitly calculated in Section III C 3 while the calculation of the 3-String diagram in Fig. 6b is outlined in Section III C 4⁵, with their double-log divergence given in Eqs. (93) and (114) (note that they are identically the same).

3. Benz Diagram

Let us briefly sketch the calculation of the Benz diagram. Before the calculation, we mention that rearranging the order in which photon propagators attach to fermion loops results in a “twin” diagram of the Benz diagram (see Fig. 7), which is simply the nested diagram of the 3-loop fermion self-energy diagram in Fig. 3c together with a single fermion loop. It only gives divergence to the Landau damping term $|k_\tau|/|k_y|$ that is canceled by the second diagram in Fig. 6d involving counterterms corresponding to fermion field strength renormalization. Similarly, the $|k_\tau|/|k_y|$ divergence of the Benz diagram is canceled by the first diagram in Fig. 6d involving counterterms corresponding to vertex renormalization, which can be explicitly checked.

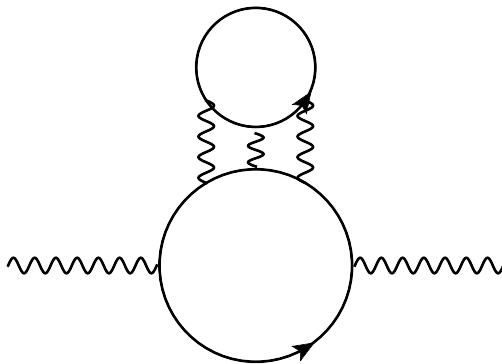


FIG. 7: The twin diagram of the Benz diagram after rearranging the order photon propagators attach to the fermion loop.

⁴ When we apply the Callan-Symanzik equation (6) to the third leading order of $1/N$, $\mu \frac{\partial}{\partial \mu}$ acted on these two diagrams involving counterterms is nonzero, yet it is cancelled by $\gamma_z k_\tau \frac{\partial}{\partial k_\tau}$ acted on AL diagram.

⁵ See also Ref. [7] for the calculation of 3-String diagram with quadratic boson kinetic term, i.e. at $\epsilon = 1$, where some $(\ln \frac{\Lambda_y}{k_y})^5$ divergence is identified.

Considering different directions fermions in the loops of Benz diagram can travel as well as different patches the fermions can belong to, there are altogether 16 different contributions from the Benz diagram, which we temporarily denote as $\Pi_{\text{Benz}} = \sum(\Pi_{\pm, C/A; \pm, C/A})$, where $\Pi_{+C, -A}$ represents the Benz diagram whose outer fermion loop lies on the + patch and runs in the clockwise (C) direction, while the inner fermion loop lies on the - patch and runs in the anti-clockwise (A) direction, etc. Unless the two fermion loops belong to the opposite patches, the diagram vanishes [3, 10]. Since the photon propagator is independent of the x -component momentum k_x , it is convenient to take $k_x = 0$, and it is then straightforward to see that simultaneously flipping the patch labels of the two fermion loops does not change the result of the diagram, i.e., $\Pi_{+C, -A} = \Pi_{-C, +A}$, etc. Furthermore, simultaneously flipping the directions in which fermions run in the two loops will complex conjugate the result, i.e., $\Pi_{+A, -C} = \Pi_{+C, -A}^*$. Therefore, the sum of all Benz diagrams can be written as

$$4\text{Re}(\Pi_{+C, -C} + \Pi_{+C, -A}). \quad (61)$$

Therefore, only two cases need to be considered : we can first set the outer loop fermion to be in the + patch travelling clockwise, while the inner loop fermion is set to be in the - patch travelling either clockwise (case *a*) or anti-clockwise (case *b*), corresponding to $\Pi_{+C, -C}$ and $\Pi_{+C, -A}$ respectively.

The Benz diagram in the two cases read

$$\begin{aligned} \Pi_{\text{Benz}}^a(k) &= \lambda_+^5 \lambda_-^3 \int [dl_1][dl_2][dp][dq] G_+(q)G_+(q+k)G_+(q+k-l_1)G_+(q-l_1)G_+(q-l_2) \\ &\quad \times G_-(p)G_-(p+l_1)G_-(p+l_2)D(l_1)D(l_2)D(l_1-l_2), \end{aligned} \quad (62)$$

$$\begin{aligned} \Pi_{\text{Benz}}^b(k) &= \lambda_+^5 \lambda_-^3 \int [dl_1][dl_2][dp][dq] G_+(q)G_+(q+k)G_+(q+k-l_1)G_+(q-l_1)G_+(q-l_2) \\ &\quad \times G_-(p)G_-(p-l_1)G_-(p-l_2)D(l_1)D(l_2)D(l_1-l_2). \end{aligned} \quad (63)$$

Using the residue theorem to calculate the integration of l_{1x} , l_{2x} , p_x , q_x , p_y and q_y in order, and taking the real part of the expression, we obtain the following expression,

$$\Pi'_{\text{Benz}}(k) \equiv \text{Re}(\Pi_{\text{Benz}}^a + \Pi_{\text{Benz}}^b) = \frac{1}{16(2\pi)^6 |k_y|} \int dl_{1\tau} dl_{1y} dl_{2\tau} dl_{2y} dp_\tau dq_\tau \left(\sum_{i=1}^6 \mathbf{B}_i \right) D(l_1)D(l_2)D(l_1-l_2), \quad (64)$$

where \mathbf{B}_i are defined as follows

$$\begin{aligned} \mathbf{B}_1 &\equiv (\theta(l_{2\tau} - q_\tau) - \theta(-l_{2\tau} - p_\tau)) (\theta(l_{1\tau} - k_\tau - q_\tau) - \theta(-l_{1\tau} - p_\tau)) (\theta(k_\tau - 2l_{1\tau} - p_\tau + q_\tau) - \theta(-p_\tau)) \\ &\quad \times (\theta(k_\tau - 2l_{1\tau} + q_\tau) - \theta(k_\tau + q_\tau)) \left(\theta \left(\frac{l_{1\tau}}{l_{1y}} \right) - \theta \left(\frac{-k_\tau + 2l_{1\tau} - 2l_{2\tau}}{2l_{1y} - 2l_{2y}} \right) \right) \\ &\quad \times \left(\theta \left(\frac{k_\tau l_{1y} + 2l_{1y} l_{2\tau} - 2l_{1\tau} l_{2y}}{2l_{1y}} \right) - \theta(k_\tau) \right) \mathcal{B}_1, \end{aligned} \quad (65)$$

$$\begin{aligned} \mathbf{B}_2 &\equiv (\theta(l_{2\tau} - q_\tau) - \theta(-l_{2\tau} - p_\tau)) (\theta(l_{1\tau} - k_\tau - q_\tau) - \theta(-l_{1\tau} - p_\tau)) (\theta(-2l_{2\tau} - p_\tau + q_\tau) - \theta(-p_\tau)) \\ &\quad \times (\theta(-2l_{2\tau} + q_\tau) - \theta(k_\tau + q_\tau)) \left(\theta \left(\frac{-k_\tau + 2l_{1\tau} - 2l_{2\tau}}{2l_{1y} - 2l_{2y}} \right) - \theta \left(\frac{k_\tau + 2l_{2\tau}}{2l_{2y}} \right) \right) \\ &\quad \times \left(\theta \left(\frac{k_\tau l_{1y} + 2l_{1y} l_{2\tau} - 2l_{1\tau} l_{2y}}{2l_{1y}} \right) - \theta(k_\tau) \right) \mathcal{B}_1, \end{aligned} \quad (66)$$

$$\begin{aligned} \mathbf{B}_3 &\equiv (\theta(l_{2\tau} - q_\tau) - \theta(-l_{2\tau} - p_\tau)) (\theta(l_{1\tau} - k_\tau - q_\tau) - \theta(-l_{1\tau} - p_\tau)) (\theta(k_\tau - 2l_{1\tau} - p_\tau + q_\tau) - \theta(-p_\tau)) \\ &\quad \times (\theta(k_\tau - 2l_{1\tau} + q_\tau) - \theta(q_\tau)) \left(\theta \left(\frac{-k_\tau + 2l_{1\tau} - 2l_{2\tau}}{2l_{1y} - 2l_{2y}} \right) - \theta \left(\frac{-k_\tau + 2l_{1\tau}}{2l_{1y}} \right) \right) \\ &\quad \times \left(\theta \left(\frac{k_\tau l_{2y} + 2l_{1y} l_{2\tau} - 2l_{1\tau} l_{2y}}{2l_{2y}} \right) - \theta(k_\tau) \right) \mathcal{B}_2, \end{aligned} \quad (67)$$

$$\begin{aligned} \mathbf{B}_4 &\equiv (\theta(l_{2\tau} - q_\tau) - \theta(-l_{2\tau} - p_\tau)) (\theta(l_{1\tau} - k_\tau - q_\tau) - \theta(-l_{1\tau} - p_\tau)) (\theta(-2l_{2\tau} - p_\tau + q_\tau) - \theta(-p_\tau)) \\ &\quad \times (\theta(-2l_{2\tau} + q_\tau) - \theta(q_\tau)) \left(\theta \left(\frac{l_{2\tau}}{l_{2y}} \right) - \theta \left(\frac{-k_\tau + 2l_{1\tau} - 2l_{2\tau}}{2l_{1y} - 2l_{2y}} \right) \right) \\ &\quad \times \left(\theta \left(\frac{k_\tau l_{2y} + 2l_{1y} l_{2\tau} - 2l_{1\tau} l_{2y}}{2l_{2y}} \right) - \theta(k_\tau) \right) \mathcal{B}_2, \end{aligned} \quad (68)$$

$$\begin{aligned}
\mathcal{B}_5 &\equiv (\theta(l_{2\tau} - q_\tau) - \theta(-l_{2\tau} - p_\tau)) (\theta(l_{1\tau} - q_\tau) - \theta(-l_{1\tau} - p_\tau)) (\theta(-2l_{1\tau} - p_\tau + q_\tau) - \theta(-p_\tau)) \\
&\quad \times (\theta(-2l_{1\tau} + q_\tau) - \theta(k_\tau + q_\tau)) \left(\theta \left(\frac{l_{1\tau} - l_{2\tau}}{l_{1y} - l_{2y}} \right) - \theta \left(\frac{k_\tau + 2l_{1\tau}}{2l_{1y}} \right) \right) \\
&\quad \times \left(\theta \left(\frac{k_\tau(l_{1y} - l_{2y}) + 2l_{1y}l_{2\tau} - 2l_{1\tau}l_{2y}}{2(l_{1y} - l_{2y})} \right) - \theta(k_\tau) \right) \mathcal{B}_3,
\end{aligned} \tag{69}$$

$$\begin{aligned}
\mathcal{B}_6 &\equiv (\theta(l_{2\tau} - q_\tau) - \theta(-l_{2\tau} - p_\tau)) (\theta(l_{1\tau} - q_\tau) - \theta(-l_{1\tau} - p_\tau)) (\theta(-2l_{2\tau} - p_\tau + q_\tau) - \theta(-p_\tau)) \\
&\quad \times (\theta(-2l_{2\tau} + q_\tau) - \theta(k_\tau + q_\tau)) \left(\theta \left(\frac{k_\tau + 2l_{2\tau}}{2l_{2y}} \right) - \theta \left(\frac{l_{1\tau} - l_{2\tau}}{l_{1y} - l_{2y}} \right) \right) \\
&\quad \times \left(\theta \left(\frac{k_\tau(l_{1y} - l_{2y}) + 2l_{1y}l_{2\tau} - 2l_{1\tau}l_{2y}}{2(l_{1y} - l_{2y})} \right) - \theta(k_\tau) \right) \mathcal{B}_3,
\end{aligned} \tag{70}$$

and $\mathcal{B}_i = \mathcal{B}_i^a - \mathcal{B}_i^b$ are defined as follows

$$\begin{aligned}
\mathcal{B}_1^a &\equiv \frac{l_{1y} ((l_{1y}l_{2\tau} - l_{1\tau}l_{2y})^2 + k_y^2 l_{1y}^2 l_{2y} (l_{1y} - l_{2y}))}{((l_{1y}l_{2\tau} - l_{1\tau}l_{2y})^2 + k_y^2 l_{1y}^2 l_{2y}^2) ((l_{1y}l_{2\tau} - l_{1\tau}l_{2y})^2 + k_y^2 l_{1y}^2 (l_{1y} - l_{2y})^2)}, \\
\mathcal{B}_2^a &\equiv \frac{l_{2y}}{(l_{1y}l_{2\tau} - l_{1\tau}l_{2y})^2 + k_y^2 l_{1y}^2 l_{2y}^2}, \\
\mathcal{B}_3^a &\equiv \frac{l_{1y} - l_{2y}}{(l_{1y}l_{2\tau} - l_{1\tau}l_{2y})^2 + k_y^2 l_{1y}^2 (l_{1y} - l_{2y})^2},
\end{aligned} \tag{71}$$

$$\begin{aligned}
\mathcal{B}_1^b &\equiv \frac{l_{1y} ((l_{1y}l_{2\tau} - l_{1\tau}l_{2y})^2 - (l_{1y}l_{2y}^2 - l_{1y}^2 l_{2y} + k_y l_{1y} l_{2y})) (l_{1y}l_{2y}^2 - l_{1y}^2 l_{2y} - k_y l_{1y} (l_{1y} - l_{2y}))}{((l_{1y}l_{2\tau} - l_{1\tau}l_{2y})^2 + (l_{1y}l_{2y}^2 - l_{1y}^2 l_{2y} + k_y l_{1y} l_{2y})^2) ((l_{1y}l_{2\tau} - l_{1\tau}l_{2y})^2 + (l_{1y}l_{2y}^2 - l_{1y}^2 l_{2y} - k_y l_{1y} (l_{1y} - l_{2y}))^2)}, \\
\mathcal{B}_2^b &\equiv \frac{l_{2y} ((l_{1y}l_{2\tau} - l_{1\tau}l_{2y})^2 - (l_{1y}l_{2y}^2 - l_{1y}^2 l_{2y}) (l_{1y}l_{2y}^2 - l_{1y}^2 l_{2y} + k_y l_{1y} l_{2y}))}{((l_{1y}l_{2\tau} - l_{1\tau}l_{2y})^2 + (l_{1y}l_{2y}^2 - l_{1y}^2 l_{2y})^2) ((l_{1y}l_{2\tau} - l_{1\tau}l_{2y})^2 + (l_{1y}l_{2y}^2 - l_{1y}^2 l_{2y} + k_y l_{1y} l_{2y})^2)}, \\
\mathcal{B}_3^b &\equiv \frac{(l_{1y} - l_{2y}) ((l_{1y}l_{2\tau} - l_{1\tau}l_{2y})^2 - (l_{1y}l_{2y}^2 - l_{1y}^2 l_{2y}) (l_{1y}l_{2y}^2 - l_{1y}^2 l_{2y} - k_y l_{1y} (l_{1y} - l_{2y})))}{((l_{1y}l_{2\tau} - l_{1\tau}l_{2y})^2 + (l_{1y}l_{2y}^2 - l_{1y}^2 l_{2y})^2) ((l_{1y}l_{2\tau} - l_{1\tau}l_{2y})^2 + (l_{1y}l_{2y}^2 - l_{1y}^2 l_{2y} - k_y l_{1y} (l_{1y} - l_{2y}))^2)}.
\end{aligned} \tag{72}$$

Note that $\mathcal{B}_1^a = \mathcal{B}_2^a + \mathcal{B}_3^a$ and $\mathcal{B}_1^b = \mathcal{B}_2^b + \mathcal{B}_3^b$.

Setting $k_\tau = 0$, we obtain

$$\begin{aligned}
\sum_{i=1}^6 \mathcal{B}_i &= \left(\hat{T}_1 \theta \left(\frac{l_{1\tau}}{l_{1y}} \right) - \hat{T}_2 \theta \left(\frac{l_{2\tau}}{l_{2y}} \right) + (\hat{T}_2 - \hat{T}_1) \theta \left(\frac{l_{1\tau} - l_{2\tau}}{l_{1y} - l_{2y}} \right) \right) (\theta(l_{1y}) - \theta(l_{2y})) \operatorname{sgn}(l_{1y}l_{2\tau} - l_{1\tau}l_{2y}) \mathcal{B}_2 \\
&\quad + (l_1 \rightarrow -l_1, \quad l_2 \rightarrow l_2 - l_1),
\end{aligned} \tag{73}$$

where the second term denotes the expression coming from transforming the first expression accordingly and the simplification comes from the left-right flipping symmetry of the Benz diagram. Here $\hat{T}_{1,2}$ are defined as follows

$$\begin{aligned}
\hat{T}_1 &\equiv (\theta(l_{2\tau} - q_\tau) - \theta(-l_{2\tau} - p_\tau)) (\theta(l_{1\tau} - q_\tau) - \theta(-l_{1\tau} - p_\tau)) \\
&\quad (\theta(-2l_{1\tau} - p_\tau + q_\tau) - \theta(-p_\tau)) (\theta(-2l_{1\tau} + q_\tau) - \theta(q_\tau)),
\end{aligned} \tag{74}$$

$$\begin{aligned}
\hat{T}_2 &\equiv (\theta(l_{2\tau} - q_\tau) - \theta(-l_{2\tau} - p_\tau)) (\theta(l_{1\tau} - q_\tau) - \theta(-l_{1\tau} - p_\tau)) \\
&\quad (\theta(-2l_{2\tau} - p_\tau + q_\tau) - \theta(-p_\tau)) (\theta(-2l_{2\tau} + q_\tau) - \theta(q_\tau)).
\end{aligned} \tag{75}$$

Then the first term and the second term should give the same contribution to $\Pi^{a,b}$, and therefore we focus on the first term. We can now explicitly see that $\Pi^{a,b}$ are even functions of k_y , as expected.

Following the procedure outlined in Section III C 1, we expand \mathcal{B}_2^a at small k_y and focus on terms proportional to k_y^2 ,

$$\mathcal{B}_2^a \rightarrow - \frac{l_{1y}^2 l_{2y}^3}{(l_{1y}l_{2\tau} - l_{1\tau}l_{2y})^2 ((l_{1y}l_{2\tau} - l_{1\tau}l_{2y})^2 + k_y^2 l_{1y}^2 l_{2y}^2)} k_y^2 \xrightarrow{f(k_y=0) \cdot k_y^2} - \frac{l_{1y}^2 l_{2y}^3}{(l_{1y}l_{2\tau} - l_{1\tau}l_{2y})^4} k_y^2. \tag{76}$$

We will just use the expression $f(0)k_y^2$ for most of our calculation, yet the full expression is important in identifying the dynamically generated IR cutoff for calculating the coefficient of the double-log. For \mathcal{B}_2^b , since only single-log is present, we just write down the expression of $f(0)k_y^2$ here for simplicity,

$$\mathcal{B}_2^b \rightarrow l_{1y}^2 l_{2y}^3 \left(- \frac{1}{((l_{1y}l_{2\tau} - l_{1\tau}l_{2y})^2 + (l_{1y}l_{2y}^2 - l_{1y}^2 l_{2y})^2)^2} + \frac{8(l_{1y}l_{2y}^2 - l_{1y}^2 l_{2y})^2}{((l_{1y}l_{2\tau} - l_{1\tau}l_{2y})^2 + (l_{1y}l_{2y}^2 - l_{1y}^2 l_{2y})^2)^3} \right. \\ \left. - \frac{8(l_{1y}l_{2y}^2 - l_{1y}^2 l_{2y})^4}{((l_{1y}l_{2\tau} - l_{1\tau}l_{2y})^2 + (l_{1y}l_{2y}^2 - l_{1y}^2 l_{2y})^2)^4} \right) k_y^2. \quad (77)$$

Note that the relevant terms in $\sum_{i=1}^6 \mathbf{B}_i$ are invariant if we simultaneously flip the sign of l_{1y} , l_{2y} or $l_{1\tau}$, $l_{2\tau}$. Therefore, let us restrict to the integration region where $l_{1y} > 0$ as well as $l_{1\tau} > 0$. In this regime, the first term of $\sum_{i=1}^6 \mathbf{B}_i$ is nonzero only when $l_{2y} < 0$ and $l_{2\tau} > 0$, and after integrating over p_τ and q_τ it becomes $\mathcal{B}_2 \times \min(l_{1\tau}, l_{2\tau})^2$. Now we are left with the integral over $l_{1\tau}$, l_{1y} , and $l_{2\tau}$ and l_{2y} . To perform this integral, first consider the region where $l_{1\tau} > l_{2\tau}$. In order to isolate the divergence, we change the integration variables as

$$l_{2y} = -l_{1y}\delta, \quad l_{1\tau} = l_{1y}^2 \Delta_1, \quad l_{2\tau} = l_{1y}^2 \Delta_2. \quad (78)$$

After the integration of δ , $\Delta_{1,2}$ as well as l_{1y} , we have the following logarithmic divergent piece of $\Sigma^{a,b}$ coming from the first term in $\sum_{i=1}^6 \mathbf{B}_i$ in the region $l_{1y} > 0$, $l_{2y} < 0$, $l_{1\tau} > l_{2\tau} > 0$,

$$\frac{|k_y|}{e^2} \frac{\alpha^4}{4\pi^2} \left(\int \frac{dl_{1y}}{l_{1y}} \int_0^\infty d\delta \int_0^\infty d\Delta_1 \int_0^{\Delta_1} d\Delta_2 \Delta_2^2 \delta^3 (\omega^a - \omega^b) \frac{1}{1 + \alpha\Delta_1} \frac{\delta}{\delta^2 + \alpha\Delta_2} \frac{1 + \delta}{(1 + \delta)^2 + \alpha(\Delta_1 - \Delta_2)} \right) \quad (79)$$

where ω^a and ω^b comes from \mathcal{B}_2^a and \mathcal{B}_2^b respectively,

$$\omega^a = \frac{1}{(\Delta_2 + \delta\Delta_1)^2 ((\Delta_2 + \delta\Delta_1)^2 + (k_y/l_{1y})^2 \delta^2)} \xrightarrow{k_y=0} \frac{1}{(\Delta_2 + \delta\Delta_1)^4}, \quad (80)$$

$$\omega^b = \frac{1}{((\delta^2 + \delta)^2 + (\Delta_2 + \delta\Delta_1)^2)^2} - \frac{8(\delta^2 + \delta)^2}{((\delta^2 + \delta)^2 + (\Delta_2 + \delta\Delta_1)^2)^3} + \frac{8(\delta^2 + \delta)^4}{((\delta^2 + \delta)^2 + (\Delta_2 + \delta\Delta_1)^2)^4}. \quad (81)$$

Next consider the region where $l_{2\tau} > l_{1\tau}$. To compare two regions let us do the following change of parameters in this region:

$$l_{2y} = -|l_{1y}|, \quad l_{1y} = |l_{1y}|\delta, \quad l_{1\tau} = l_{1y}^2 \Delta_2, \quad l_{2\tau} = l_{1y}^2 \Delta_1. \quad (82)$$

The logarithmic divergent piece in this region is then written as follows,

$$\frac{|k_y|}{e^2} \frac{\alpha^4}{4\pi^2} \left(\int \frac{dl_{1y}}{l_{1y}} \int_0^\infty d\delta \int_0^\infty d\Delta_1 \int_0^{\Delta_1} d\Delta_2 \Delta_2^2 \delta^2 (\omega^a - \omega^b) \frac{1}{1 + \alpha\Delta_1} \frac{\delta}{\delta^2 + \alpha\Delta_2} \frac{1 + \delta}{(1 + \delta)^2 + \alpha(\Delta_1 - \Delta_2)} \right) \quad (83)$$

Adding the contribution of all regions up is now straightforward, which is simply adding Eqs. (79) and (83) before multiplied by 4. The second term in $\sum_{i=1}^6 \mathbf{B}_i$ gives an extra factor of 2 while different directions in which fermions travel as well as different fermion patch numbers give an extra factor of 4. Carefully considering all these factors, the Benz diagram gives the following log divergent contribution to boson self-energy

$$4\Pi'_{\text{Benz}}(k) \rightarrow \frac{|k_y|}{e^2} \frac{8\alpha^4}{\pi^2} \int \frac{dl_{1y}}{l_{1y}} (M^a(\alpha) - M^b(\alpha)), \quad (84)$$

where $M_{a,b}(\alpha)$ are defined as

$$M^{a,b}(\alpha) \equiv \int_0^\infty d\delta \int_0^\infty d\Delta_1 \int_0^{\Delta_1} d\Delta_2 \Delta_2^2 \delta^2 (1 + \delta) \omega^{a,b} \frac{1}{1 + \alpha\Delta_1} \frac{\delta}{\delta^2 + \alpha\Delta_2} \frac{1 + \delta}{(1 + \delta)^2 + \alpha(\Delta_1 - \Delta_2)} \quad (85)$$

with $\omega^{a,b}$ defined in Eqs. (80) and (81). At $k_y = 0$, even though $M^b(\alpha)$ is just a regular function of α , $M^a(\alpha)$ is not, because of the divergent integration coming from the region where Δ_1 and Δ_2 go to zero simultaneously, which can be translated to the dynamical region where

$$|l_{1y}|, |l_{2y}| \gg |k_y|, \quad |l_{1\tau}|, |l_{2\tau}| \approx |k_y l_{1y}|. \quad (86)$$

Note that $|k_y l_{1y}|$ is approximately the on-shell energy of a fermion with x -momentum l_{1y}^2 and y -momentum $k_y + l_{1y}$. Therefore the integral is actually double-log divergent instead of single-log divergent. Denoting the integrand of $M^a(\alpha)$ as $m^a(\alpha)$, we separate $M^a(\alpha)$ in the following way

$$\begin{aligned}
M^a(\alpha) &\equiv \int_0^\infty d\delta \int_0^\infty d\Delta_1 \int_0^{\Delta_1} d\Delta_2 m^a(\alpha) \\
&= \left(\int_0^\infty d\delta \int_1^\infty d\Delta_1 \int_0^{\Delta_1} d\Delta_2 m^a(\alpha) \right) \\
&+ \left(\int_0^\infty d\delta \int_0^1 d\Delta_1 \int_0^{\Delta_1} d\Delta_2 \left(m^a(\alpha) - \frac{\Delta_2^2 \delta}{(\Delta_2 + \delta \Delta_1)^2 ((\Delta_2 + \delta \Delta_1)^2 + (k_y/l_{1y})^2 \delta^2)} \right) \right) \\
&+ \left(\int_0^\infty d\delta \int_0^1 d\Delta_1 \int_0^{\Delta_1} d\Delta_2 \frac{\Delta_2^2 \delta}{(\Delta_2 + \delta \Delta_1)^2 ((\Delta_2 + \delta \Delta_1)^2 + (k_y/l_{1y})^2 \delta^2)} \right).
\end{aligned} \tag{87}$$

Then only the third term is IR divergent at $k_y = 0$, which will be related to the double-log divergence we are after.

In order to compute the coefficient of the double-log through the *expansion trick* sketched in Section III C 1, we need to first identify the IR cutoff for l_τ and l_y . For this, we return to the full expression of the integrand,

$$\int_0^{\Lambda_y} dl_{1y} \int_0^{\Lambda_y} dl_{2y} \int_0^{l_{1y}^2} dl_{1\tau} \int_0^{l_{1\tau}} dl_{2\tau} \frac{l_{2\tau}^2 l_{1y} l_{2y}}{(l_{1y} l_{2\tau} - l_\tau l_{2y})^2 ((l_{1y} l_{2\tau} - l_\tau l_{2y})^2 + k_y^2 l_{1y}^2 l_{2y}^2)}. \tag{88}$$

From Eq. (76) or (88), the crossover scale appears when $(l_{1y} l_{2\tau} - l_\tau l_{2y})^2$ is of the same order as $k_y^2 l_{1y}^2 l_{2y}^2$, and therefore the dynamically generated IR cutoff for l_τ should be $k_y l_y$. Again, note that $|k_y l_{1y}|$ is approximately the on-shell energy of a fermion with x -momentum l_{1y}^2 and y -momentum $k_y + l_{1y}$. Accordingly, we can do the integration of Δ_1 from k_y/l_{1y} instead of 0 to 1, which gives us a log term. This log term is reminiscent of the BCS-log associated to the real Cooper pair [11, 12], which is also tied solely to the integration of frequency, and hence looks like a virtual BCS-log. Then the third term after the integration of $\delta, \Delta_1, \Delta_2$ as well as l_{1y} is

$$\int \frac{dl_{1y}}{l_{1y}} M^a(\alpha) \rightarrow \frac{1}{6} \int_{k_y}^{\Lambda_y} \frac{dl_{1y}}{l_{1y}} \int_{k_y/l_{1y}}^1 \frac{d\Delta_1}{\Delta_1} = \frac{1}{12} \left(\ln \left(\frac{\Lambda_y}{k_y} \right) \right)^2. \tag{89}$$

It is also possible to calculate the coefficient of the relevant double-log divergent terms explicitly. Here, it is possible to do the explicit integration. After integrating over Δ_1, Δ_2 and δ , the result is a function $f(k_y/l_{1y})$, explicitly written out as follows,

$$f(x) = \frac{x((x^2 + 3) \ln(x^2 + 1) - 2x^2 \ln(x) - 4) + 4 \arctan(x)}{12x^3}. \tag{90}$$

and the third term now becomes $\int \frac{dl_{1y}}{l_{1y}} f\left(\frac{k_y}{l_{1y}}\right)$. From the limiting behavior of $f(x)$ at small and large x ,

$$f(x) = \begin{cases} -\frac{1}{6} \ln(x) & x \ll 1 \\ \frac{1}{2} \frac{\ln(x)}{x^2} & x \gg 1 \end{cases} \tag{91}$$

we see that the integration $\int \frac{dx}{x} f\left(\frac{1}{x}\right)$ is IR convergent and UV double-log divergent. Hence the integration of l_{1y} is IR convergent and UV double-log divergent. This integration can be carried out explicitly as well, which at large Λ_y/k_y is

$$\frac{1}{12} \left(\ln \left(\frac{\Lambda_y}{k_y} \right) \right)^2 + \frac{5}{36} \ln \left(\frac{\Lambda_y}{k_y} \right) + \frac{3\pi^2 + 38}{432}. \tag{92}$$

The double-log term in (92) agrees with Eq. (89) that is obtained from the simplified scheme. This yields the promised double-log divergent term

$$\Pi_{\text{Benz}}(k) \rightarrow \frac{|k_y|}{e^2} \frac{2\alpha^4}{3\pi^2} \left(\ln \left(\frac{\Lambda_y}{k_y} \right) \right)^2. \tag{93}$$

4. 3-String Diagram

Finally, let us briefly sketch the calculation of the 3-String diagram. For simplicity, we focus on the case where $k_\tau = 0$ whenever possible. As in previous cases, the two fermion loops must belong to different patches to give rise to UV divergence. Since the photon propagator is independent of the x -component momentum k_x , we can set the left fermion loop to be in the $-$ patch without loss of generality. We can also fix that fermion in the left loop runs in counterclockwise direction and fermion in the right loop runs in clockwise direction. Then there are 6 possible ways in which the three internal photon propagators attach to the two loops, shown in Fig. 8. After simultaneously flipping the directions in which fermions run in the two loops, diagram a and b do not change, while c, d and e, f transform into each other respectively. Therefore, the contribution of the 3-String diagram as a whole becomes

$$2(\Pi^a + \Pi^b) + 4\text{Re}(\Pi^c + \Pi^e), \quad (94)$$

where

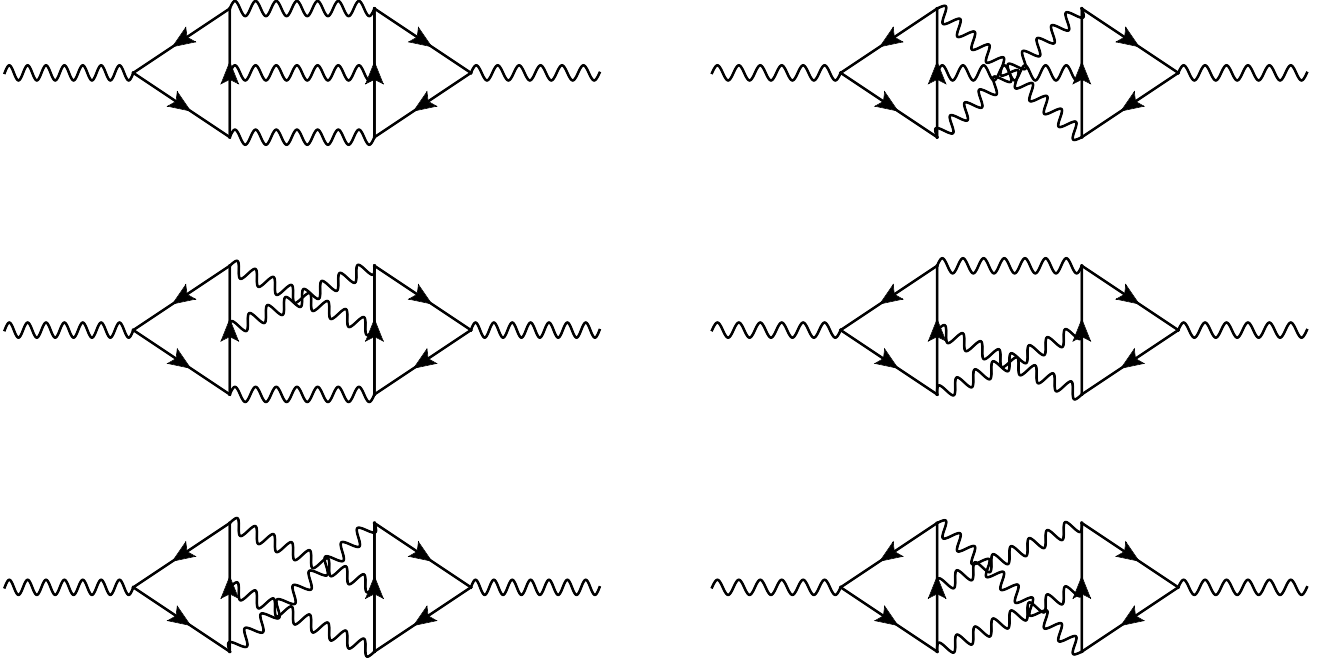


FIG. 8: All possible 3-String diagrams depending on how three internal photon propagators attach to the fermion loops. From left to right then from top down are case a, b, c, d, e and f respectively.

$$\begin{aligned} \Pi_{3\text{String}}^a(k) &= \lambda_+^4 \lambda_-^4 \int [dl_1][dl_2][dp][dq] G_-(p)G_-(p+k)G_-(p+l_1+k/2)G_-(p+l_2+k/2) \\ &\quad \times G_+(q)G_+(q-k)G_+(q-l_1-k/2)G_+(q-l_2-k/2)D(k/2+l_1)D(k/2-l_2)D(l_1-l_2), \end{aligned} \quad (95)$$

$$\begin{aligned} \Pi_{3\text{String}}^b(k) &= \lambda_+^4 \lambda_-^4 \int [dl_1][dl_2][dp][dq] G_-(p)G_-(p+k)G_-(p+l_1+k/2)G_-(p+l_2+k/2) \\ &\quad \times G_+(q)G_+(q+k)G_+(q+l_1+k/2)G_+(q+l_2+k/2)D(k/2+l_1)D(k/2-l_2)D(l_1-l_2), \end{aligned} \quad (96)$$

$$\begin{aligned} \Pi_{3\text{String}}^c(k) &= \lambda_+^4 \lambda_-^4 \int [dl_1][dl_2][dp][dq] G_-(p)G_-(p+k)G_-(p+l_1+k/2)G_-(p+l_2+k/2) \\ &\quad \times G_+(q)G_+(q+l_1+k/2)G_+(q+l_2+k/2)G_+(q+l_2-k/2)D(k/2+l_1)D(k/2-l_2)D(l_1-l_2), \end{aligned} \quad (97)$$

$$\begin{aligned} \Pi_{3\text{String}}^e(k) &= \lambda_+^4 \lambda_-^4 \int [dl_1][dl_2][dp][dq] G_-(p)G_-(p+k)G_-(p+l_1+k/2)G_-(p+l_2+k/2) \\ &\quad \times G_+(q)G_+(q-l_1-k/2)G_+(q-l_2-k/2)G_+(q-l_2+k/2)D(k/2+l_1)D(k/2-l_2)D(l_1-l_2). \end{aligned} \quad (98)$$

Again, we use the residue theorem to calculate the integration of l_{1x} , l_{2x} , p_x , q_x , p_y and q_y in order. The expression at non-zero k_τ is extremely lengthy, but there is some simplification when $k_\tau = 0$:

$$\Pi_{3\text{String}}^{a,b,c,e}(k_y) = \frac{\text{sgn}(k_y)}{(2\pi)^6 |k_y|} \int dl_{1\tau} dl_{1y} dl_{2\tau} dl_{2y} dp_\tau dq_\tau \left(-\hat{T}_1 \mathcal{S}_1^{a,b,c,e} + \hat{T}_2 \mathcal{S}_2^{a,b,c,e} \right) D(k/2 + l_1) D(k/2 - l_2) D(l_2 - l_1) \quad (99)$$

where $\hat{T}_{1,2}$ are defined in (74) and (75) and

$$\begin{aligned} \mathcal{S}_i^{a,b} \equiv & \left(\theta \left(\frac{2l_{i\tau}}{2l_{iy} - k_y} \right) - \theta \left(\frac{2l_{i\tau}}{2l_{iy} + k_y} \right) \right) \left(\theta \left(\frac{2l_{i\tau}}{2l_{iy} - k_y} \right) \mathcal{S}_{i,-}^{a,b} - \theta \left(\frac{2l_{i\tau}}{2l_{iy} + k_y} \right) \mathcal{S}_{i,+}^{a,b} \right) \\ & + \left(\theta \left(\frac{2l_{i\tau}}{2l_{iy} - k_y} \right) - \theta \left(\frac{l_{1\tau} - l_{2\tau}}{l_{1y} - l_{2y}} \right) \right) \theta \left(\frac{k_y(l_{1\tau} - l_{2\tau}) + 2l_{1y}l_{2\tau} - 2l_{1\tau}l_{2y}}{k_y(l_{1y} - l_{2y})} \right) \\ & - \left(\theta \left(\frac{2l_{i\tau}}{2l_{iy} + k_y} \right) - \theta \left(\frac{l_{1\tau} - l_{2\tau}}{l_{1y} - l_{2y}} \right) \right) \theta \left(\frac{k_y(l_{1\tau} - l_{2\tau}) - 2l_{1y}l_{2\tau} + 2l_{1\tau}l_{2y}}{k_y(l_{1y} - l_{2y})} \right) \mathcal{S}_0^{a,b}, \end{aligned} \quad (100)$$

$$\begin{aligned} \mathcal{S}_1^{c,e} \equiv & \left(\theta \left(\frac{2l_{1\tau}}{2l_{1y} - k_y} \right) - \theta \left(\frac{2l_{1\tau}}{2l_{1y} + k_y} \right) \right) \theta \left(\frac{2l_{1\tau}}{2l_{1y} + k_y} \right) \mathcal{S}_1^{c,e} \\ & + \left(\theta \left(\frac{2l_{1\tau}}{2l_{1y} + k_y} \right) - \theta \left(\frac{l_{1\tau} - l_{2\tau}}{l_{1y} - l_{2y}} \right) \right) \theta \left(\frac{k_y(l_{1\tau} - l_{2\tau}) - 2l_{1y}l_{2\tau} + 2l_{1\tau}l_{2y}}{k_y(2l_{1y} + k_y)} \right) \mathcal{S}_1^{c,e} \\ & - \left(\theta \left(\frac{2l_{1\tau}}{2l_{1y} - k_y} \right) - \theta \left(\frac{l_{1\tau} - l_{2\tau}}{l_{1y} - l_{2y}} \right) \right) \theta \left(\frac{k_y(l_{1\tau} - l_{2\tau}) + 2l_{1y}l_{2\tau} - 2l_{1\tau}l_{2y}}{k_y(-2l_{2y} + k_y)} \right) \mathcal{S}_2^{c,e} \\ & + \theta \left(\frac{k_y(l_{1\tau} - l_{2\tau}) + 2l_{1y}l_{2\tau} - 2l_{1\tau}l_{2y}}{k_y(l_{1y} - l_{2y})} \right) \mathcal{S}_0^{c,e}, \end{aligned} \quad (101)$$

$$\begin{aligned} \mathcal{S}_2^{c,e} \equiv & \left(\theta \left(\frac{2l_{2\tau}}{2l_{2y} + k_y} \right) - \theta \left(\frac{2l_{2\tau}}{2l_{2y} - k_y} \right) \right) \left(\theta \left(\frac{2l_{2\tau}}{2l_{2y} - k_y} \right) \mathcal{S}_{2,-}^{c,e} - \theta \left(\frac{2l_{2\tau}}{2l_{2y} + k_y} \right) \mathcal{S}_{2,+}^{c,e} \right) \\ & + \left(\theta \left(\frac{2l_{2\tau}}{2l_{2y} + k_y} \right) - \theta \left(\frac{l_{1\tau} - l_{2\tau}}{l_{1y} - l_{2y}} \right) \right) \theta \left(\frac{k_y(l_{1\tau} - l_{2\tau}) - 2l_{1y}l_{2\tau} + 2l_{1\tau}l_{2y}}{k_y(2l_{1y} + k_y)} \right) \mathcal{S}_1^{c,e} \\ & - \left(\theta \left(\frac{2l_{2\tau}}{2l_{2y} - k_y} \right) - \theta \left(\frac{l_{1\tau} - l_{2\tau}}{l_{1y} - l_{2y}} \right) \right) \theta \left(\frac{k_y(l_{1\tau} - l_{2\tau}) + 2l_{1y}l_{2\tau} - 2l_{1\tau}l_{2y}}{k_y(-2l_{2y} + k_y)} \right) \mathcal{S}_2^{c,e} \\ & + \theta \left(\frac{k_y(l_{1\tau} - l_{2\tau}) + 2l_{1y}l_{2\tau} - 2l_{1\tau}l_{2y}}{k_y(l_{1y} - l_{2y})} \right) \mathcal{S}_0^{c,e}, \end{aligned} \quad (102)$$

where the most important \mathcal{S} factors for case *a* are defined as follows,

$$\begin{aligned} \mathcal{S}_{i,\pm}^a & \equiv \frac{k_y \pm 2l_{iy}}{16k_y l_{i\tau} (k_y(l_{1\tau} - l_{2\tau}) \mp 2(l_{1y}l_{2\tau} - l_{1\tau}l_{2y}))}, \\ \mathcal{S}_0^a & \equiv \frac{l_{1y} - l_{2y}}{4(k_y(l_{1\tau} - l_{2\tau}) + 2l_{1y}l_{2\tau} - 2l_{1\tau}l_{2y})(k_y(l_{1\tau} - l_{2\tau}) - 2l_{1y}l_{2\tau} + 2l_{1\tau}l_{2y})}, \end{aligned} \quad (103)$$

and for case *b*,

$$\begin{aligned} \mathcal{S}_{i,\pm}^b & \equiv (k_y \pm 2l_{iy}) \left/ \left\{ 2k_y (4l_{i\tau} - i(k_y^2 - 4l_{iy}^2)) \right. \right. \\ & \quad \times \left. \left. (2(k_y(l_{1\tau} - l_{2\tau}) \mp 2(l_{1y}l_{2\tau} - l_{1\tau}l_{2y})) \pm i(k_y^2(l_{1y} - l_{2y}) + 4(l_{1y}^2 l_{2y} - l_{2y}^2 l_{1y})) + 2ik_y(l_{1y}^2 - l_{2y}^2)) \right\}, \right. \\ & \quad (104) \\ \mathcal{S}_0^b & \equiv (l_{1y} - l_{2y}) \left/ \left\{ (2(k_y(l_{1\tau} - l_{2\tau}) + 2(l_{1y}l_{2\tau} - l_{1\tau}l_{2y})) - i(k_y^2(l_{1y} - l_{2y}) + 4(l_{1y}^2 l_{2y} - l_{2y}^2 l_{1y})) + 2ik_y(l_{1y}^2 - l_{2y}^2)) \right. \right. \\ & \quad \times \left. \left. (2(k_y(l_{1\tau} - l_{2\tau}) - 2(l_{1y}l_{2\tau} - l_{1\tau}l_{2y})) + i(k_y^2(l_{1y} - l_{2y}) + 4(l_{1y}^2 l_{2y} - l_{2y}^2 l_{1y})) + 2ik_y(l_{1y}^2 - l_{2y}^2)) \right\}, \right. \end{aligned}$$

and for case c ,

$$\begin{aligned}
\mathcal{S}_1^c &\equiv (-k_y - 2l_{1y}) \left/ \left\{ 2 \left(k_y^2 l_{1y} - k_y^2 l_{2y} - 2ik_y l_{1\tau} + 2k_y l_{1y}^2 + 2ik_y l_{2\tau} - 2k_y l_{2y}^2 - 4il_{1\tau} l_{2y} + 4l_{1y}^2 l_{2y} + 4il_{1y} l_{2\tau} - 4l_{1y} l_{2y}^2 \right) \right. \right. \\
&\quad \left. \left. \times \left(k_y^2 l_{1y} - k_y^2 l_{2y} - 2ik_y l_{1\tau} + 2k_y l_{1y}^2 - 4k_y l_{1y} l_{2y} - 2ik_y l_{2\tau} + 2k_y l_{2y}^2 + 4il_{1\tau} l_{2y} - 4l_{1y}^2 l_{2y} - 4il_{1y} l_{2\tau} + 4l_{1y} l_{2y}^2 \right) \right\}, \right. \\
\mathcal{S}_2^c &\equiv (-k_y + 2l_{2y}) \left/ \left\{ 2 \left(-k_y^2 l_{1y} + k_y^2 l_{2y} + 2ik_y l_{1\tau} - 2k_y l_{1y}^2 + 4k_y l_{1y} l_{2y} - 2ik_y l_{2\tau} - 2k_y l_{2y}^2 - 4il_{1\tau} l_{2y} + 4l_{1y}^2 l_{2y} + 4il_{1y} l_{2\tau} - 4l_{1y} l_{2y}^2 \right) \right. \right. \\
&\quad \left. \left. \times \left(-k_y^2 l_{1y} + k_y^2 l_{2y} + 2ik_y l_{1\tau} - 2k_y l_{1y}^2 + 4k_y l_{1y} l_{2y} + 2ik_y l_{2\tau} - 2k_y l_{2y}^2 - 4il_{1\tau} l_{2y} + 4l_{1y}^2 l_{2y} + 4il_{1y} l_{2\tau} - 4l_{1y} l_{2y}^2 \right) \right\}, \right. \\
\mathcal{S}_0^c &= \mathcal{S}_1^c - \mathcal{S}_2^c \equiv (-l_{1y} + l_{2y}) \left/ \left\{ \left(k_y^2 l_{1y} - k_y^2 l_{2y} - 2ik_y l_{1\tau} + 2k_y l_{1y}^2 + 2ik_y l_{2\tau} - 2k_y l_{2y}^2 - 4il_{1\tau} l_{2y} + 4l_{1y}^2 l_{2y} + 4il_{1y} l_{2\tau} - 4l_{1y} l_{2y}^2 \right) \right. \right. \\
&\quad \left. \left. \times \left(k_y^2 l_{1y} - k_y^2 l_{2y} - 2ik_y l_{1\tau} + 2k_y l_{1y}^2 - 4k_y l_{1y} l_{2y} + 2ik_y l_{2\tau} + 2k_y l_{2y}^2 + 4il_{1\tau} l_{2y} - 4l_{1y}^2 l_{2y} - 4il_{1y} l_{2\tau} + 4l_{1y} l_{2y}^2 \right) \right\}, \right. \\
\mathcal{S}_{2,-}^c &\equiv i(k_y - 2l_{2y}) \left/ \left\{ 8k_y l_{2\tau} \left(-k_y^2 l_{1y} + k_y^2 l_{2y} + 2ik_y l_{1\tau} - 2k_y l_{1y}^2 + 4k_y l_{1y} l_{2y} + 2ik_y l_{2\tau} - 2k_y l_{2y}^2 - 4il_{1\tau} l_{2y} + 4l_{1y}^2 l_{2y} + 4il_{1y} l_{2\tau} - 4l_{1y} l_{2y}^2 \right) \right\}, \right. \\
\mathcal{S}_{2,+}^c &\equiv i(k_y + 2l_{2y}) \left/ \left\{ 8k_y l_{2\tau} \left(-k_y^2 l_{1y} + k_y^2 l_{2y} + 2ik_y l_{1\tau} - 2k_y l_{1y}^2 - 2ik_y l_{2\tau} + 2k_y l_{2y}^2 + 4il_{1\tau} l_{2y} - 4l_{1y}^2 l_{2y} - 4il_{1y} l_{2\tau} + 4l_{1y} l_{2y}^2 \right) \right\}, \right.
\end{aligned} \tag{105}$$

and, finally, for case e ,

$$\begin{aligned}
\mathcal{S}_1^e &\equiv i(k_y + 2l_{1y}) \left/ \left\{ 4(k_y l_{1\tau} - k_y l_{2\tau} + 2l_{1\tau} l_{2y} - 2l_{1y} l_{2\tau}) \right. \right. \\
&\quad \left. \left. \times \left(2k_y^2 l_{1y} - 2k_y^2 l_{2y} + k_y^3 + 2ik_y l_{1\tau} - 4k_y l_{1y} l_{2y} + 2ik_y l_{2\tau} - 4il_{1\tau} l_{2y} + 4il_{1y} l_{2\tau} \right) \right\}, \right. \\
\mathcal{S}_2^e &\equiv (k_y - 2l_{2y}) \left/ \left\{ 4 \left(-k_y^2 l_{1y} + k_y^2 l_{2y} - ik_y l_{1\tau} + 2k_y l_{1y} l_{2y} + ik_y l_{2\tau} - 2k_y l_{2y}^2 + 2il_{1\tau} l_{2y} - 2il_{1y} l_{2\tau} \right) \right. \right. \\
&\quad \left. \left. \times \left(2k_y^2 l_{1y} - 2k_y^2 l_{2y} + k_y^3 + 2ik_y l_{1\tau} - 4k_y l_{1y} l_{2y} + 2ik_y l_{2\tau} - 4il_{1\tau} l_{2y} + 4il_{1y} l_{2\tau} \right) \right\}, \right. \\
\mathcal{S}_0^e &= \mathcal{S}_1^e - \mathcal{S}_2^e \equiv -i(l_{1y} - l_{2y}) \left/ \left\{ 4(k_y l_{1\tau} - k_y l_{2\tau} + 2l_{1\tau} l_{2y} - 2l_{1y} l_{2\tau}) \right. \right. \\
&\quad \left. \left. \times \left(-k_y^2 l_{1y} + k_y^2 l_{2y} - ik_y l_{1\tau} + 2k_y l_{1y} l_{2y} + ik_y l_{2\tau} - 2k_y l_{2y}^2 + 2il_{1\tau} l_{2y} - 2il_{1y} l_{2\tau} \right) \right\}, \right. \\
\mathcal{S}_{2,-}^e &\equiv (-k_y + 2l_{2y}) \left/ \left\{ 2k_y \left(k_y^2 + 4il_{2\tau} - 4l_{2y}^2 \right) \right. \right. \\
&\quad \left. \left. \times \left(2k_y^2 l_{1y} - 2k_y^2 l_{2y} + k_y^3 + 2ik_y l_{1\tau} - 4k_y l_{1y} l_{2y} + 2ik_y l_{2\tau} - 4il_{1\tau} l_{2y} + 4il_{1y} l_{2\tau} \right) \right\}, \right. \\
\mathcal{S}_{2,+}^e &\equiv i(k_y + 2l_{2y}) \left/ \left\{ 4k_y \left(k_y^2 + 4il_{2\tau} - 4l_{2y}^2 \right) \left(k_y l_{1\tau} - k_y l_{2\tau} - 2l_{1y} l_{2\tau} + 2l_{1\tau} l_{2y} \right) \right\}. \right.
\end{aligned} \tag{106}$$

First consider case a and b . Because of the theta pre-factors, only $\mathcal{S}_0^{a,b}$ contribute to UV divergence according to the *local divergence conjecture* in Section III C 1. Setting $k_y = 0$ everywhere in the theta factors except for an overall $\text{sgn}(k_y)$, we obtain

$$-\hat{T}_1 \mathcal{S}_1^{a,b} + \hat{T}_2 \mathcal{S}_2^{a,b} \approx \left(-\hat{T}_1 \theta \left(\frac{l_{1\tau}}{l_{1y}} \right) + \hat{T}_2 \theta \left(\frac{l_{2\tau}}{l_{2y}} \right) + (\hat{T}_1 - \hat{T}_2) \theta \left(\frac{l_{1\tau} - l_{2\tau}}{l_{1y} - l_{2y}} \right) \right) \text{sgn} \left(\frac{l_{1y} l_{2\tau} - l_{1\tau} l_{2y}}{k_y (l_{1y} - l_{2y})} \right) \mathcal{S}_0^{a,b}. \tag{107}$$

Again the real part of this expression is invariant if we simultaneously flip the sign of k_y, l_{1y}, l_{2y} or $l_{1\tau}, l_{2\tau}$.

Therefore let us assume $l_{1\tau} > 0$ as well as $l_{1y} > 0$. Then we have six regions where the expression is non-zero,

$$\begin{aligned}
\text{region 1:} \quad & l_{2\tau} > l_{1\tau} > 0, \quad l_{1y} > l_{2y} > 0, \quad \int dp_\tau dq_\tau \left(-\hat{T}_1 \mathcal{S}_1^{a,b} + \hat{T}_2 \mathcal{S}_2^{a,b} \right) = -(l_{2\tau} - l_{1\tau})^2 \text{sgn}(k_y) \mathcal{S}_0^{a,b}, \\
\text{region 2:} \quad & l_{2\tau} > l_{1\tau} > 0, \quad l_{2y} < 0, \quad \int dp_\tau dq_\tau \left(-\hat{T}_1 \mathcal{S}_1^{a,b} + \hat{T}_2 \mathcal{S}_2^{a,b} \right) = -l_{1\tau}^2 \text{sgn}(k_y) \mathcal{S}_0^{a,b}, \\
\text{region 3:} \quad & l_{1\tau} > l_{2\tau} > 0, \quad l_{2y} > l_{1y} > 0, \quad \int dp_\tau dq_\tau \left(-\hat{T}_1 \mathcal{S}_1^{a,b} + \hat{T}_2 \mathcal{S}_2^{a,b} \right) = (l_{2\tau} - l_{1\tau})^2 \text{sgn}(k_y) \mathcal{S}_0^{a,b}, \\
\text{region 4:} \quad & l_{1\tau} > l_{2\tau} > 0, \quad l_{2y} < 0, \quad \int dp_\tau dq_\tau \left(-\hat{T}_1 \mathcal{S}_1^{a,b} + \hat{T}_2 \mathcal{S}_2^{a,b} \right) = -l_{2\tau}^2 \text{sgn}(k_y) \mathcal{S}_0^{a,b}, \\
\text{region 5:} \quad & l_{2\tau} < 0, \quad l_{2y} > l_{1y} > 0, \quad \int dp_\tau dq_\tau \left(-\hat{T}_1 \mathcal{S}_1^{a,b} + \hat{T}_2 \mathcal{S}_2^{a,b} \right) = l_{1\tau}^2 \text{sgn}(k_y) \mathcal{S}_0^{a,b}, \\
\text{region 6:} \quad & l_{2\tau} < 0, \quad l_{1y} > l_{2y} > 0, \quad \int dp_\tau dq_\tau \left(-\hat{T}_1 \mathcal{S}_1^{a,b} + \hat{T}_2 \mathcal{S}_2^{a,b} \right) = -l_{2\tau}^2 \text{sgn}(k_y) \mathcal{S}_0^{a,b}.
\end{aligned} \tag{108}$$

After interchanging $l_{1\tau}, l_{2\tau}$ as well as l_{1y}, l_{2y} simultaneously, we see that the expressions in region 1 and 3, 2 and 4, as well as 5 and 6 are identical to each other respectively, and therefore we can focus on region 1, 2 and 5. The analysis of case c and e are straightforward as well. Because of the theta pre-factors, $\mathcal{S}_{2,\pm}^{c,e}$ do not contribute to the divergence in the UV. Setting $k_y = 0$ everywhere in the theta factors except for an overall $\text{sgn}(k_y)$, we obtain

$$\begin{aligned}
-\hat{T}_1 \mathcal{S}_1^{c,e} + \hat{T}_2 \mathcal{S}_2^{c,e} &\approx \left(-\hat{T}_1 \theta \left(\frac{l_{1\tau}}{l_{1y}} \right) + \hat{T}_2 \theta \left(\frac{l_{2\tau}}{l_{2y}} \right) + (\hat{T}_1 - \hat{T}_2) \theta \left(\frac{l_{1\tau} - l_{2\tau}}{l_{1y} - l_{2y}} \right) \right) \\
&\quad \times \text{sgn}(l_{1y} l_{2\tau} - l_{1\tau} l_{2y}) \text{sgn}(k_y) \left(\theta(-l_{1y}) \mathcal{S}_1^{c,e} - \theta(-l_{2y}) \mathcal{S}_2^{c,e} - \theta(l_{1y} - l_{2y}) \mathcal{S}_0^{c,e} \right).
\end{aligned} \tag{109}$$

Restricting to the regime where $l_{1y} > 0$ as well as $l_{1\tau} > 0$, we have four different sections on the $l_{2y} - l_{2\tau}$ plane where the expression is non-zero,

$$\begin{aligned}
\text{region 1:} \quad & l_{2\tau} > l_{1\tau} > 0, \quad l_{1y} > l_{2y} > 0, \quad \int dp_\tau dq_\tau \left(-\hat{T}_1 \mathcal{S}_1^{c,e} + \hat{T}_2 \mathcal{S}_2^{c,e} \right) = (l_{2\tau} - l_{1\tau})^2 \text{sgn}(k_y) \mathcal{S}_0^{c,e}, \\
\text{region 2:} \quad & l_{2\tau} > l_{1\tau} > 0, \quad l_{2y} < 0, \quad \int dp_\tau dq_\tau \left(-\hat{T}_1 \mathcal{S}_1^{c,e} + \hat{T}_2 \mathcal{S}_2^{c,e} \right) = l_{1\tau}^2 \text{sgn}(k_y) \mathcal{S}_1^{c,e}, \\
\text{region 4:} \quad & l_{1\tau} > l_{2\tau} > 0, \quad l_{2y} < 0, \quad \int dp_\tau dq_\tau \left(-\hat{T}_1 \mathcal{S}_1^{c,e} + \hat{T}_2 \mathcal{S}_2^{c,e} \right) = l_{2\tau}^2 \text{sgn}(k_y) \mathcal{S}_1^{c,e}, \\
\text{region 6:} \quad & l_{2\tau} < 0, \quad l_{1y} > l_{2y} > 0, \quad \int dp_\tau dq_\tau \left(-\hat{T}_1 \mathcal{S}_1^{c,e} + \hat{T}_2 \mathcal{S}_2^{c,e} \right) = l_{2\tau}^2 \text{sgn}(k_y) \mathcal{S}_0^{c,e}.
\end{aligned} \tag{110}$$

The expression for single log divergence is very involved, but it is manageable to calculate the double log divergence as sketched in Section III C 1. First, we expand the whole expression in powers of k_y . As in the calculation of the Benz diagram, we collect terms at the third order in the expansion, i.e. terms proportional to k_y^2 . Note that k_y mainly appears in two different places, in \mathcal{S} factors as well as in $D(k/2 + l_1)D(k/2 - l_2)^6$. To simplify expressions further, we are allowed to set $k_y = 0$ inside the boson propagators except for the case c and region 2 and 4 of case e , where we have to take into account the second term in the expansion of both $\mathcal{S}_1^{c,e}$ and $D(k/2 + l_1)D(k/2 - l_2)$ at small k_y , i.e. terms proportional to k_y in two terms respectively ⁷.

For the sake of presentation, let us first identify the double log divergence coming from the dynamical region (86)⁸. We just need to collect terms at the third order of the expansion that are proportional to $1/l_\tau^4$ and contribute to the IR divergence in the integration of $l_{1\tau}, l_{2\tau}$. These terms only come from case e , hence we write down the terms proportional to k_y in the series expansion of \mathcal{S}^e ,

$$\begin{aligned}
\mathcal{S}_0^e \Big|_{k_y \text{ linear term}} &= \left(\frac{l_{2y}^2 (l_{1y} - l_{2y})^3}{16(l_{1y} l_{2\tau} - l_{1\tau} l_{2y})^4} - \frac{(l_{1y} - l_{2y})(l_{1\tau} - l_{2\tau})^2}{64(l_{1y} l_{2\tau} - l_{1\tau} l_{2y})^4} \right) k_y^2, \\
\mathcal{S}_1^e \Big|_{k_y \text{ linear term}} &= \left(\frac{l_{2y}^2 l_{1y}^3}{16(l_{1y} l_{2\tau} - l_{1\tau} l_{2y})^4} - \frac{l_{1y}(l_{1\tau}^2 + l_{2\tau}^2) + 2l_{2y} l_{1\tau} l_{2\tau}}{64(l_{1y} l_{2\tau} - l_{1\tau} l_{2y})^4} \right) k_y^2.
\end{aligned} \tag{111}$$

⁶ k_y also appears in theta factors, but there it only contributes to a shift of integration regions in the IR that we can ignore for the calculation in the UV.

⁷ Expanding \mathcal{S} factors at small k_y , symbolically we have $\mathcal{S} \approx x_0 + x_1 k_y + x_2 k_y^2$. Moreover, $D(k/2 + l_1)D(k/2 - l_2) \approx d_0 + d_1 k_y + d_2 k_y^2$. We can explicitly check that the integration of $x_0 d_0$, i.e. the constant term, is cancelled among the six cases. The same calculation also shows that the integration of $x_0 d_2$ is cancelled among the six cases. What we now have are $x_2 d_0$ as well as $x_1 d_1$. We then notice that $x_1 = 0$ expect for $\mathcal{S}_{0,1}^c$ and \mathcal{S}_1^e .

⁸ Here we need to distinguish between integration region 1-6, and dynamical region on the boundary of respective integration region that contributes mostly to the double log divergence.

We see that k_y -linear terms of \mathcal{S}^e are separated into two terms $\mathcal{S}^{e,(1)} + \mathcal{S}^{e,(2)}$. The first terms $\mathcal{S}^{e,(1)}$ of the two expansions are proportional to $1/l_\tau^4$ while the second terms $\mathcal{S}^{e,(2)}$ are not, and we isolate the first terms,

$$\begin{aligned}\mathcal{S}_1^{e,(1)} &= \frac{l_{1y}^3 l_{2y}^2}{16(l_{1y}l_{2\tau} - l_{1\tau}l_{2y})^4} k_y^2, \\ \mathcal{S}_2^{e,(1)} &= \frac{l_{2y}^3 (l_{2y}^2 - 3l_{1y}l_{2y} + 3l_{1y}^2)}{16(l_{1y}l_{2\tau} - l_{1\tau}l_{2y})^4} k_y^2, \\ \mathcal{S}_0^{e,(1)} &= \frac{l_{2y}^2 (l_{1y} - l_{2y})^3}{16(l_{1y}l_{2\tau} - l_{1\tau}l_{2y})^4} k_y^2.\end{aligned}\tag{112}$$

Just considering these terms coming from case e , we see that, to our surprise, Eq. (109) becomes identical to Eq. (73) after interchanging $l_{1\tau}, l_{1y}$ with $l_{2\tau}, l_{2y}$. Namely, after substituting \mathcal{S}^e in (109) with $\mathcal{S}^{e,(1)}$ and interchanging label $l_{1\tau}, l_{1y}$ and $l_{2\tau}, l_{2y}$, we have

$$\begin{aligned}\left(-\hat{T}_1 \mathcal{S}_1^e + \hat{T}_2 \mathcal{S}_2^e\right)^{(1)} &= \frac{\text{sgn}(k_y) k_y^2}{16} \left(\hat{T}_1 \theta\left(\frac{l_{1\tau}}{l_{1y}}\right) - \hat{T}_2 \theta\left(\frac{l_{2\tau}}{l_{2y}}\right) + (\hat{T}_2 - \hat{T}_1) \theta\left(\frac{l_{1\tau} - l_{2\tau}}{l_{1y} - l_{2y}}\right) \right) \\ &\times \left(-(\theta(l_{1y}) - \theta(l_{2y})) \text{sgn}(l_{1y}l_{2\tau} - l_{1\tau}l_{2y}) \frac{l_{1y}^2 l_{2y}^3}{(l_{1y}l_{2\tau} - l_{1\tau}l_{2y})^4} + (l_1 \rightarrow -l_1, \quad l_2 \rightarrow l_2 - l_1) \right),\end{aligned}\tag{113}$$

which is identical to the expression we obtain after substituting (76) into (73), except for an extra factor $\frac{\text{sgn}(k_y)}{16}$ which can be accounted for from different factors in front of the whole expression as shown in (64) and (99). Moreover, both contribute to photon self-energy with an extra factor of 4 as shown in (61) and (94). Therefore, we calculate the double log divergence of the 3-String diagram originating from the same source as the Benz diagram, i.e. coming from the dynamical region Eq. (86),

$$\Pi_{3\text{String}}(k) \rightarrow \frac{|k_y|}{e^2} \frac{2\alpha^4}{3\pi^2} \left(\ln\left(\frac{\Lambda_y}{k_y}\right) \right)^2.\tag{114}$$

After subtracting these terms out, now we aim to show that the double log divergences of the rest of the 3-String diagram cancel among the six cases. These double-log divergences that are canceled among themselves come from dynamical regions with large $l_{1\tau}$ or $l_{2\tau}$. The UV divergences from these high-energy modes can only renormalize local terms in the action. As a result, both single-log and double-log, which require non-local counter terms, are expected to be canceled. One interesting conclusion we can draw from this surprising result is that the double log divergence actually does not appear at this order in the $\epsilon = 0$ version of Ising-nematic transition in a metal [1], which is very closely related to the nFL theory we discussed here except $\lambda_+ = \lambda_- = +1$. Here $\lambda_+ = \lambda_-$ because the critical Ising-nematic order parameter, which is the analog of the field a discussed here, couples to a fermion bilinear operator whose symmetry form factor requires $\lambda_+ = \lambda_-$.

Let us do the calculation in region 4 of case e as an example. To unearth the double-log divergence from the second term in the expansion (111), we do the following change of parameters:

$$l_{2y} = -l_{1y}\delta, \quad l_{1\tau} = l_{1y}^2 \Delta_1, \quad l_{2\tau} = l_{1y}^2 \Delta_2,\tag{115}$$

and integrate $|l_{1y}|$ from k_y to Λ_y . The logarithmic divergent piece in this region from the second term is then written as follows,

$$\begin{aligned}(\Pi^e(k))^{(2)} \Big|_{\text{region 4}} &\approx \frac{|k_y|}{(2\pi)^6} \int_0^\infty dl_{1y} \int_{-\infty}^0 dl_{2y} \int_0^\infty dl_{1\tau} \int_0^{l_{1\tau}} dl_{2\tau} l_{2\tau}^2 \mathcal{S}_1^{e,(2)} D(k/2 + l_1) D(k/2 - l_2) D(l_2 - l_1) \\ &= -\frac{|k_y|}{e^2} \frac{\alpha^4}{16\pi^2} \left(\int \frac{dl_{1y}}{l_{1y}} \int_0^\infty d\delta \int_0^\infty d\Delta_1 \int_0^{\Delta_1} d\Delta_2 \frac{\Delta_2^2 (\Delta_1^2 + \Delta_2^2 + 2\delta\Delta_1\Delta_2)}{(\Delta_2 + \delta\Delta_1)^4} \right. \\ &\quad \left. \times \frac{1}{1 + \alpha\Delta_1} \frac{\delta}{\delta^2 + \alpha\Delta_2} \frac{1 + \delta}{(1 + \delta)^2 + \alpha(\Delta_1 - \Delta_2)} \right).\end{aligned}\tag{116}$$

The above integration is IR divergent when Δ_2 and δ go to zero simultaneously, which can be translated to the dynamical region where

$$|l_{1y}| \gg |k_y|, \quad |l_{1\tau}| \gg |k_y l_{1y}|, \quad |l_{2y}| \approx |k_y|, \quad |l_{2\tau}| \approx |k_y l_{1y}|.\tag{117}$$

To simplify the expression further, we change Δ_2 to $\Delta'_2\delta$, then at small δ the integrand is approximately

$$\frac{\Delta'_2\Delta_1^2}{\alpha(\Delta_1 + \Delta'_2)^4(1 + \alpha\Delta_1)^2} \frac{1}{\delta}, \quad (118)$$

which gives the following double log divergence in the bracket

$$\frac{1}{6\alpha^2} \int_{k_y}^{\Lambda_y} \frac{dl_{1y}}{l_{1y}} \int_{k_y/l_{1y}}^1 \frac{d\delta}{\delta} = \frac{1}{12\alpha^2} \left(\ln \left(\frac{\Lambda_y}{k_y} \right) \right)^2. \quad (119)$$

The calculation in the other integration regions and other cases are as straightforward, and we see that the double-log divergent terms in region 2, 4, 5 and 6 of case *a* and *b* are all the same, i.e.

$$\Pi^{a,b}(k) \Big|_{\text{region 2,4,5,6}} \rightarrow \frac{|k_y|}{e^2} \frac{\alpha^2}{192\pi^2} \left(\ln \left(\frac{\Lambda_y}{k_y} \right) \right)^2, \quad (120)$$

while the double log divergent terms in region 4 and 6 of case *c* and the second term of *e* are all the same, i.e.

$$\Pi^c(k), (\Pi^e(k))^{(2)} \Big|_{\text{region 4,6}} \rightarrow - \frac{|k_y|}{e^2} \frac{\alpha^2}{192\pi^2} \left(\ln \left(\frac{\Lambda_y}{k_y} \right) \right)^2, \quad (121)$$

and in all the other regions there is no additional double log divergence. Adding them all up we see that the additional double log divergence cancels among the six cases, as promised.

It is worth pointing out that the calculation of the 3-String diagram relies on the ‘‘local divergence conjecture’’ we make in Section III C 1 as well as the correctness of the expansion trick with correct dynamically generated IR cutoff. It will be very interesting if a more rigorous calculation of these coefficients, either analytically or numerically, can be done. We defer this to future work.

-
- [1] Max A. Metlitski and Subir Sachdev, ‘‘Quantum phase transitions of metals in two spatial dimensions. I. Ising-nematic order,’’ *Phys. Rev. B* **82**, 075127 (2010), arXiv:1001.1153 [cond-mat.str-el].
 - [2] Sung-Sik Lee, ‘‘Stability of the U(1) spin liquid with a spinon Fermi surface in 2+1 dimensions,’’ *Phys. Rev. B* **78**, 085129 (2008), arXiv:0804.3800 [cond-mat.str-el].
 - [3] Sung-Sik Lee, ‘‘Low-energy effective theory of Fermi surface coupled with U(1) gauge field in 2+1 dimensions,’’ *Phys. Rev. B* **80**, 165102 (2009), arXiv:0905.4532 [cond-mat.str-el].
 - [4] David F. Mross, John McGreevy, Hong Liu, and T. Senthil, ‘‘Controlled expansion for certain non-Fermi-liquid metals,’’ *Phys. Rev. B* **82**, 045121 (2010), arXiv:1003.0894 [cond-mat.str-el].
 - [5] Liujun Zou and Debanjan Chowdhury, ‘‘Deconfined metallic quantum criticality: A U(2) gauge-theoretic approach,’’ *Physical Review Research* **2**, 023344 (2020), arXiv:2002.02972 [cond-mat.str-el].
 - [6] Liujun Zou and Debanjan Chowdhury, ‘‘Deconfined Metal-Insulator Transitions in Quantum Hall Bilayers,’’ *Physical Review Research* **2**, 032071 (2020), arXiv:2004.14391 [cond-mat.str-el].
 - [7] Tobias Holder and Walter Metzner, ‘‘Anomalous dynamical scaling from nematic and U(1) gauge field fluctuations in two-dimensional metals,’’ *Phys. Rev. B* **92**, 041112 (2015), arXiv:1503.05089 [cond-mat.str-el].
 - [8] Tobias Holder and Walter Metzner, ‘‘Fermion loops and improved power-counting in two-dimensional critical metals with singular forward scattering,’’ *Phys. Rev. B* **92**, 245128 (2015), arXiv:1509.07783 [cond-mat.str-el].
 - [9] L. G. Aslamazov and A. I. Larkin, ‘‘Effect of Fluctuations on the Properties of a Superconductor Above the Critical Temperature - Sov. Phys. Solid State 10, 875 (1968),’’ in *30 Years of the Landau Institute*, Vol. 11, edited by Isaak M. Khalatnikov and Vladimir P. Mineev (1996) p. 23.
 - [10] Shouvik Sur and Sung-Sik Lee, ‘‘Chiral non-Fermi liquids,’’ *Phys. Rev. B* **90**, 045121 (2014), arXiv:1310.7543 [cond-mat.str-el].
 - [11] Joseph Polchinski, ‘‘Effective Field Theory and the Fermi Surface,’’ arXiv e-prints, hep-th/9210046 (1992), arXiv:hep-th/9210046 [hep-th].
 - [12] R. Shankar, ‘‘Renormalization-group approach to interacting fermions,’’ *Reviews of Modern Physics* **66**, 129–192 (1994), arXiv:cond-mat/9307009 [cond-mat].